01 Aug 2018

Dynamics of Paramagnetic and Ferromagnetic Ellipsoidal Particles in Shear Flow under a Uniform Magnetic Field

Christopher A. Sobecki

Jie Zhang

Yanzhi Zhang
Missouri University of Science and Technology, zhangyanz@mst.edu

Cheng Wang
Missouri University of Science and Technology, wancheng@mst.edu

Recommended Citation

C. A. Sobecki et al., "Dynamics of Paramagnetic and Ferromagnetic Ellipsoidal Particles in Shear Flow under a Uniform Magnetic Field," *Physical Review Fluids*, vol. 3, no. 8, American Physical Society (APS), Aug 2018.
The definitive version is available at https://doi.org/10.1103/PhysRevFluids.3.084201

Dynamics of paramagnetic and ferromagnetic ellipsoidal particles in shear flow under a uniform magnetic field

Christopher A. Sobecki,[1] Jie Zhang,[1] Yanzhi Zhang,[2] and Cheng Wang[1,*]
[1]*Department of Mechanical and Aerospace Engineering, Missouri University of Science and Technology, Rolla, Missouri 65409, USA*
[2]*Department of Mathematics and Statistics, Missouri University of Science and Technology, Rolla, Missouri 65409, USA*

(Received 14 March 2018; published 14 August 2018)

We investigate the two-dimensional dynamic motion of magnetic particles of ellipsoidal shapes in shear flow under the influence of a uniform magnetic field. In the first part, we present a theoretical analysis of the rotational dynamics of the particles in simple shear flow. By considering paramagnetic and ferromagnetic particles, we study the effects of the direction and strength of the magnetic field on the particle rotation. The critical magnetic-field strength, at which particle rotation is impeded, is determined. In a weak-field regime (i.e., below the critical strength) where the particles execute complete rotations, the symmetry property of the rotational velocity is shown to depend on the direction of the magnetic field. In a strong-field regime (i.e., above the critical strength), the particles are impeded at steady angles and the stability of these angles is examined. Under a uniform field, paramagnetic and ferromagnetic particles behave differently, in terms of the critical strength, symmetry property of the rotational velocity, and steady angles. In the second part, we use two-dimensional numerical simulations to study the implications of rotational dynamics for lateral migration of the particles in wall-bound shear flows. In the weak-field regime, the paramagnetic prolate particles migrate away when the field is applied perpendicular to the flow and towards the bounded wall when the field is applied parallel to the flow. Ferromagnetic particles exhibit negligible migration under fields that are parallel or perpendicular to the flow. The different lateral migration behaviors are due to the difference in the symmetry property of particle rotational velocity. In the strong-field regime, the particles are impeded at different stable steady angles, which result in different lateral migration behaviors as well. The fundamental insights from our work demonstrate various feasible strategies for manipulating paramagnetic and ferromagnetic particles.

DOI: 10.1103/PhysRevFluids.3.084201

I. INTRODUCTION

A magnetic field is commonly used to manipulate the transport of micro- and nanosize magnetic particles in a number of technological fields. For example, magnetic separations of ferromagnetic and paramagnetic particles are used in many applications, including metal manufacturing, mining, waste water treatment, food processing, biosciences, and biotechnology [1,2]. In medicine, magnetically assisted drug delivery relies on external magnetic forces to guide the transport of magnetic drug carriers to specific locations in order to enhance drug delivery efficiency [3]. The basic principle of most magnetic manipulations is to use magnetic forces to extract or retain targets of interests, e.g., ferromagnetic impurities [4], cells that have intrinsic magnetic moments [2], and diamagnetic

*wancheng@mst.edu

biological entities that are labeled with magnetic particles [2]. Generating magnetic forces requires a spatially nonuniform field, i.e., a magnetic-field gradient [1,5].

Recent experimental [6,7] and numerical studies [8,9] have demonstrated a unique way to manipulate transport behaviors of nonspherical particles by combining a uniform magnetic field and shear flows at the micrometer length scale and in the low-Reynolds-number flow regime. Although uniform fields exert no forces, a nonzero magnetic torque is able to induce a lateral migration, which results in focusing and separation of particles by their nonspherical shape. In the work of Zhou *et al.* [7], the magnetic torque breaks the symmetry of the rotational velocity of paramagnetic particles. Lateral migration of the particle is a result of the coupling of the asymmetric rotation and translation via particle-wall hydrodynamic interactions. By using numerical simulations and a far-field theory, Matsunaga *et al.* showed that it is possible to induce lateral migration of ferromagnetic particles in a strong magnetic field [8,9]. The working principle is based on the pinning of ellipsoids at a quasisteady angle, which results in a nonzero transverse motion due to the vertical component of the image stresslet caused by the wall [8,10]. In both cases, the lateral migration motions are attributed to hydrodynamic interactions between the particle and wall under the intervention of magnetic torques. The difference of lateral migration velocities is key to continuous magnetic separation in microfluidics [11].

Effective and precise manipulation of particles by using torques needs a fundamental knowledge of particle rotational dynamics in shear flows. Earlier theoretical and experimental work investigated the effect of uniform magnetic and electric fields on the rotation of ellipsoidal particles in shear flows [12–14] at zero Reynolds number. Dielectric ellipsoids, when subjected to a uniform electric field perpendicular to the flow direction, spend a longer time in the first half than in the second half of the rotation at low-field strength and they are impeded from rotation above a critical electric-field strength [12,13]. Almog and Frankel showed that a dipolar spheroid (ferromagnetic) in an unbounded simple shear flow spirals to a single orbit when subjected to a weak external torque and reaches stable orientations under a sufficiently strong torque [15].

However, there has been no study that systematically investigates the effect of magnetic properties (paramagnetic or ferromagnetic) on particle dynamics in shear flows. It is well known that paramagnetic and ferromagnetic materials exhibit different magnetic responses to external magnetic fields. For a paramagnetic particle, its magnetic moment is induced by an external magnetic field and changes with the external field while ferromagnetic particles have a permanent moment in a unique direction and remain the same under an external magnetic field. These two kinds of magnetic particles are also of most interest for practical separation applications mentioned earlier.

In the first part of this work, we investigate theoretically the rotational dynamics of prolate ellipsoidal particles, which are made of paramagnetic and ferromagnetic materials, in a three-dimensional (3D) simple shear flow at the zero-Reynolds-number limit. In our analysis, a uniform magnetic field is imposed at an arbitrary direction relative to the flow direction. We introduce dimensionless parameters S_p and S_f to characterize the relative strength between the magnetic and hydrodynamic torques. Our theory shows that the field strength S_p or S_f and field direction β dictate the rotational dynamics of the particles. Above a critical strength (or in a strong field), particle rotation is impeded at steady angles. Below the critical strength (or in a weak field), the particle is able to execute complete rotations, but the symmetry of the rotational velocity can be broken or preserved depending on the field direction and the magnetic property of the particle. In the second part of this work, we use 2D numerical simulations to demonstrate different lateral migration motions for the two kinds of particles in wall-bound shear flows resulting from their rotational dynamics. Due to different magnetic properties, there are several possible ways to separate ferromagnetic and paramagnetic particles by applying a uniform magnetic field parallel or perpendicular to the flow direction.

II. FORMULATION OF PROBLEM

As shown in Fig. 1, our analysis considers a prolate ellipsoidal particle (with semimajor axis a, semiminor axes $b = c$, and particle aspect ratio $r = a/b$) in a 3D simple shear flow $u = \dot{\gamma} z$, with

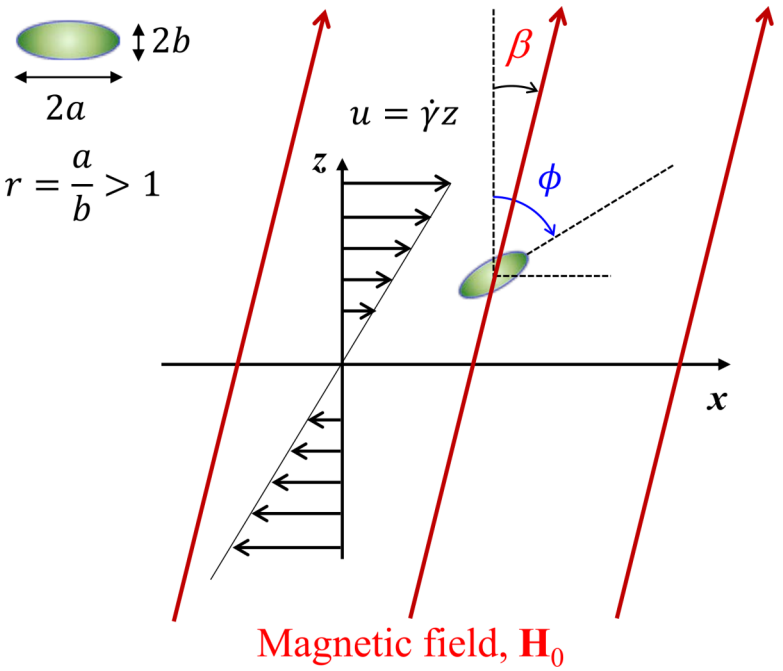

FIG. 1. Schematic of a magnetic prolate ellipsoid (major axis $2a$ and minor axis $2b = 2c$) in a simple shear flow. A uniform magnetic field is imposed at an arbitrary direction, characterized by β. The particle orientation is denoted by ϕ, and later ϕ_p and ϕ_f will be used to distinguish paramagnetic and ferromagnetic particles.

$\dot{\gamma}$ denoting the shear rate. An external magnetic field $\mathbf{H}_0 = H_0(\sin\beta, 0, \cos\beta)$ is applied parallel to the x-z plane, where H_0 denotes its magnitude and β represents the angle measured from the positive z axis as shown in Fig. 1. In this study, we restrict our analysis to the in-plane motion of the particle. The assumption of in-plane motion is justified by characteristics of typical experiment setups: (a) A static uniform magnetic field is often applied parallel to the x-z plane and (b) the particles normally have to go through a wide section of channel before entering the main fluidic channel. In those wide channel sections, the flow speed is small and allows sufficient time for the magnetic field to reorientate the long axis of ellipsoidal particles to the x-z plane. The in-plane motion was observed in our earlier work [6,7]. We assume that the particle is neutrally buoyant and the Brownian effect is negligible for micrometer-size particles. The fluid is assumed to be nonmagnetic and Newtonian with constant density ρ and dynamic viscosity η. We further assume that fluid and particle inertia is negligible (i.e., zero Reynolds number). Therefore, the hydrodynamic and magnetic torques dictate the rotational dynamics of the particles.

A. Hydrodynamic torque

In the absence of a magnetic field, the particle experiences a hydrodynamic torque due to the simple shear flow and rotates at an angular velocity $\omega_h \mathbf{e}_y$ in the x-z plane. Here ω_h is used to signify the rotation that is solely due to the hydrodynamic flow. The hydrodynamic torque acting on an ellipsoid has been derived by Okagawa *et al.* [12]. Here, by considering the rotation in the x-z plane only, we reexpress the hydrodynamic torque as $\mathbf{L}_h = L_h \mathbf{e}_y$, with its magnitude being

$$L_h = \frac{2V\eta(r^2+1)}{r^2 D_{xx} + D_{zz}}\left[\frac{\cos(2\phi)(r^2-1)}{2(r^2+1)}\dot{\gamma} + \frac{\dot{\gamma}}{2} - \dot{\phi}\right], \tag{1}$$

where $V = \frac{4}{3}\pi ab^2$ is the volume of the particle and D_{xx} and D_{yy} are the diagonal components of the demagnetizing factor. In Eq. (1), we have used relationships the $D_{xx} = 1 - A$ and $D_{zz} = A/2$, with $A = \frac{r^2}{r^2-1} - \frac{r\cosh^{-1}(r)}{(r^2-1)^{3/2}}$ for later convenience when we consider the total torque under the combined effects of the hydrodynamic flow and magnetic field. Assuming negligible particle inertia, the total torque (in this case only hydrodynamic torque) acting on the particle is zero, thereby leading to the particle angular velocity in the x-z plane, $\omega_h = \dot{\phi} = \dot{\gamma}(r^2\cos^2\phi + \sin^2\phi)/(r^2+1)$, which is the classical result from Jeffery [16]. Introducing the dimensionless time $\bar{t} = \dot{\gamma}t$ and letting $\bar{\phi}(\bar{t}) = \phi(t)$, we have

$$\dot{\phi} = \frac{r^2\cos^2\phi + \sin^2\phi}{r^2+1}. \tag{2}$$

Here and in the following we remove the overbar for notational simplicity.

B. Magnetic torque

When subjected to a uniform external magnetic field $\mathbf{H}_0$, the magnetic particle experiences a magnetic torque $\mathbf{L}_m = \mu_0(\mathbf{m} \times \mathbf{H}_0)$, where $\mathbf{m}$ is the magnetic moment of the particle and μ_0 is the magnetic permeability of vacuum. There are two common kinds of magnetic particles, paramagnetic and ferromagnetic particles, for which the origin of the magnetic moment is different. The magnetic moment $\mathbf{m}$ for a paramagnetic particle is induced by the externally applied field $\mathbf{H}_0$ and thus changes with the external field. The magnetic moment $\mathbf{m}$ of a ferromagnetic particle is an intrinsic property, i.e., it has a unique direction and magnitude, regardless of the presence of an external magnetic field. The torques caused by the external magnetic field will therefore differ for particles that have the same shape but different magnetic properties. This difference in magnetic torque has different influences on the rotational dynamics of the particles, as we will discuss in the rest of the paper.

III. PARAMAGNETIC PARTICLE

We assume that the paramagnetic particle is homogeneous and linearly magnetizable. Then the magnetic moment of the particle is $\mathbf{m} = \chi V\mathbf{H}^-$, where χ is its constant magnetic susceptibility and $\mathbf{H}^-$ is the uniform magnetic field inside the particle [17,18]. Hence, the magnetic torque on a paramagnetic particle can be written as $\mathbf{L}_{mp} = \mu_0\chi V(\mathbf{H}^- \times \mathbf{H}_0)$. In an earlier work [7], we derived the expression of magnetic torque on a paramagnetic ellipsoid suspended in a magnetic fluid in the x-z plane. Utilizing this result, we obtain the torque for a magnetic particle suspended in a nonmagnetic fluid $\mathbf{L}_{mp} = L_{mp}\mathbf{e}_y$, where L_{mp} is

$$L_{mp} = \frac{-\mu_0 V\chi^2 H_0^2 \sin(2\phi_p - 2\beta)(D_{zz} - D_{xx})}{2(1+\chi D_{xx})(1+\chi D_{zz})}. \tag{3}$$

Note that L_{mp} is a periodic function of ϕ_p with period π, due to the fore-aft symmetry of the paramagnetic ellipsoid. Thus, magnetic fields with $\beta + \pi$ or β have the same torque and effect on the particle motion.

In a quiescent fluid (i.e., $\dot{\gamma} = 0$), the magnetic torque $\mathbf{L}_{mp}$ would result in an angular velocity $\omega_{mp}\mathbf{e}_y$ of the particle with

$$\omega_{mp} = -\frac{\mu_0\chi^2 H_0^2 \sin(2\phi_p - 2\beta)}{\eta}\lambda(r,\chi), \tag{4}$$

where

$$\lambda(r,\chi) = \frac{(r^2 D_{xx} + D_{zz})(D_{zz} - D_{xx})}{4(r^2+1)(1+\chi D_{xx})(1+\chi D_{zz})}. \tag{5}$$

We now introduce a dimensionless parameter S_p, to measure the relative strength between the magnetic and hydrodynamic effects on a paramagnetic particle

$$S_p = \frac{\max_\phi\{|\omega_{mp}|\}}{\min_\phi\{|\omega_h|\}} = \frac{\mu_0\chi^2 H_0^2(r^2 D_{xx} + D_{zz})(D_{zz} - D_{xx})}{4\gamma\eta(1+\chi D_{xx})(1+\chi D_{zz})}. \tag{6}$$

That is, the parameter S_p represents the ratio between the maximum rotational speed of the particle due to the magnetic field alone in a quiescent fluid and the minimum rotational speed due to a simple shear flow alone for an inertia-free and freely rotating particle. It can also be interpreted as the ratio of magnitudes between the maximum magnetic torque [when $|\sin(2\phi - 2\beta)| = 1$] and the minimum hydrodynamic torque (when $\phi = \pi/2$ or $3\pi/2$). By definition, the parameter S_p includes the shape effect of the particles via the parameters D_{xx} and D_{zz}.

The total angular velocity of the inertia-free paramagnetic particle, due to both hydrodynamic and magnetic effects, can be determined from $\mathbf{L}_h + \mathbf{L}_{mp} = 0$. We now express the total dimensionless angular velocity of the paramagnetic particle in a dimensionless form

$$\dot{\phi}_p = \frac{r^2\cos^2\phi_p + \sin^2\phi_p - S_p\sin(2\phi_p - 2\beta)}{r^2+1}, \tag{7}$$

which is a periodic function of ϕ with period of π, since $\mathbf{L}_h$ and $\mathbf{L}_{mp}$ also have a period of π for ellipsoidal particles. Here we use ϕ_p to describe the orientation of a paramagnetic particle; ϕ_f will be used for a ferromagnetic particle in Sec. IV. Note that $S_p = 0$ when $r = 1$ and Eq. (7) will become the classical Jeffery equation. Thus, a paramagnetic sphere under a uniform magnetic field will behave just like a normal sphere as if there was no magnetic field.

A. Critical field strength $S_p^{\rm cr}$

The angular velocity of the paramagnetic particle, as in Eq. (7), indicates that the parameters S_p and β dictate the particle rotational behavior. For small S_p, the particle will be able to execute complete rotations, whereas the rotation will be impeded for sufficiently large S_p. To determine the critical field strength $S_p^{\rm cr}$, i.e., minimum field strength required to impede particle rotation, we first study the impeded steady angle(s). Setting $\dot{\phi}_p = 0$ in Eq. (7), we have determined the solutions in our earlier work [7]:

$$\tan\left(\phi_p^s\right) = \frac{S_p\cos 2\beta \pm \sqrt{S_p^2 + S_p(r^2-1)\sin 2\beta - r^2}}{1 - S_p\sin 2\beta}. \tag{8}$$

The critical field strength for the existence of the steady angle(s) to Eq. (8) is given as [7]

$$S_p^{\rm cr} = \frac{1}{2}[\sqrt{(r^2-1)^2\sin^2 2\beta + 4r^2} - (r^2-1)\sin 2\beta]. \tag{9}$$

Substituting $S_p = S_p^{\rm cr}$, we obtain the critical steady angle

$$\tan\phi_p^{\rm cr} = \frac{S_p^{\rm cr}\cos 2\beta}{1 - S_p^{\rm cr}\sin 2\beta}. \tag{10}$$

Figure 2(a) shows the value of $S_p^{\rm cr}$ as a function of β for particles with different particle aspect ratios ($r = 2$, 3, and 4). The results suggest that the field strength required to impede the particle rotation is the smallest when $\beta = \pi/4$ and the largest when $\beta = 3\pi/4$. In Fig. 2(b), when the magnetic field is applied at $\beta = 0$, the particle will first be impeded at an angle between $\pi/4$ and $\pi/2$. As β increases from 0 to $3\pi/4$, $\phi_p^{\rm cr}$ increases monotonically until $\phi_p^{\rm cr} = \pi$ when $\beta = 3\pi/4$. At $\beta = \pi/4$, $\phi_p^{\rm cr} = \pi/2$, and $\phi_p^{\rm cr} = 0$ (or π) when $\beta = 3\pi/4$. For any aspect ratio, the critical angle is always $\phi_p^{\rm cr} = \pi/2$ at $\beta = \pi/4$ and $\phi_p^{\rm cr} = 0$ (or π) when $\beta = 3\pi/4$. As β increases from $3\pi/4$ to π, the critical steady angle $\phi_p^{\rm cr}$ increases from 0 to angles between $\pi/4$ and $\pi/2$.

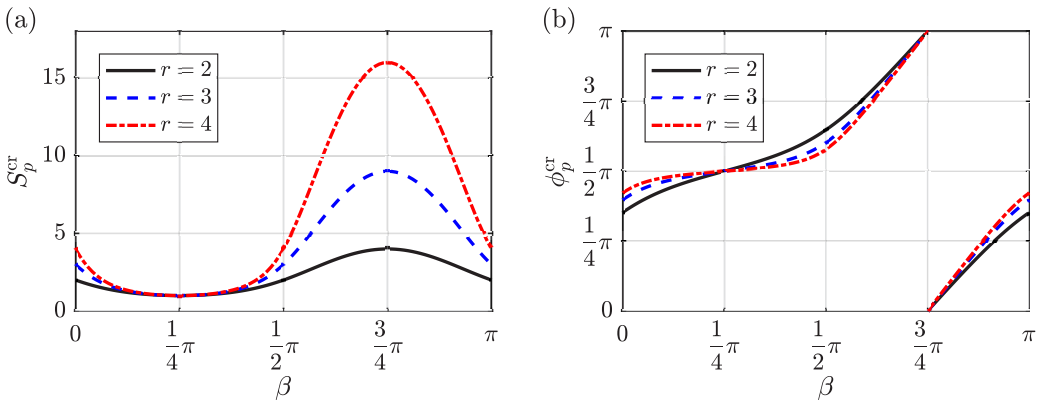

FIG. 2. (a) Critical-field strength $S_p^{\rm cr}$ and (b) critical steady angle $\phi_p^{\rm cr}$ as a function of field direction β for a paramagnetic particle with $r = 2$, 3, and 4.

B. Steady angles in the strong-field regime $S_p > S_p^{\rm cr}$

When $S_p > S_p^{\rm cr}$, the particle cannot execute complete rotations, but will be impeded at ϕ_p^s, which has two values

$$\phi_{p\pm}^s = \arctan\left[\frac{S_p\cos 2\beta \pm \sqrt{S_p^2 + S_p(r^2-1)\sin 2\beta - r^2}}{1 - S_p\sin 2\beta}\right] + k\pi, \tag{11}$$

where $k = 0$ or 1, so that $\phi_{p+}^s, \phi_{p-}^s \in [0, \pi)$. The stability of the particle's impeded angles can be determined by examining the derivative of $\frac{d\dot{\phi}_p}{d\phi_p}|_{\phi_{p\pm}^s}$. We plot the steady angles and their corresponding $\frac{d\dot{\phi}_p}{d\phi_p}$ as a function of strength for a particle with $r = 4$, when the magnetic field is applied at $\beta = 0$ and $\beta = \pi/2$, as shown in Fig. 3. (See Fig. 13 in Appendix A for $\beta = \pi/4$ and $\beta = 3\pi/4$.) As can be seen, as S_p increases above $S_p^{\rm cr}$, the two steady angles diverge from $\phi_p^{\rm cr}$: One steady angle increases while the other decreases. In the limit of an infinite-field strength, i.e., $S_p \to \infty$, the steady angle ϕ_{p-}^s approaches β, meaning that the particle's major axis is aligned with the field direction; the other steady angle ϕ_{p+}^s approaches $\beta + \pi/2$ [or $\beta - \pi/2$ if $\beta > \pi/2$ because $\beta \in (0, \pi)$], suggesting the alignment of the minor axis with the field direction. Furthermore, we find that $\frac{d\dot{\phi}_p}{d\phi_p}|_{\phi_{p+}^s} > 0$, hence ϕ_{p+}^s is always unstable, whereas $\frac{d\dot{\phi}_p}{d\phi_p}|_{\phi_{p-}^s} < 0$ and thus ϕ_{p-}^s is stable. When $S_p = S_p^{\rm cr}$, we have $\frac{d\dot{\phi}_p}{d\phi_p}|_{\phi_p^{\rm cr}} = 0$, which means that the $\phi_p^{\rm cr}$ is neutrally stable and will not be experimentally observed when disturbances are present.

C. Particle rotation in the weak-field regime $S_p < S_p^{\rm cr}$

In the weak-field regime, i.e., $S_p < S_p^{\rm cr}$, the particle rotates periodically with period π according to Eq. (7). Hence, the dimensionless period of over a rotation of 2π is $t_p^{(0,2\pi)} = 2t_p^{(0,\pi)}$. For notational simplicity, we will define the period over (s, q) as $t_i^{(s,q)} = \int_s^q d\phi_i/\dot{\phi}_i$ for any s and q, where $i = p$ for paramagnetic particles and $i = f$ for ferromagnetic particles. For paramagnetic particles, we

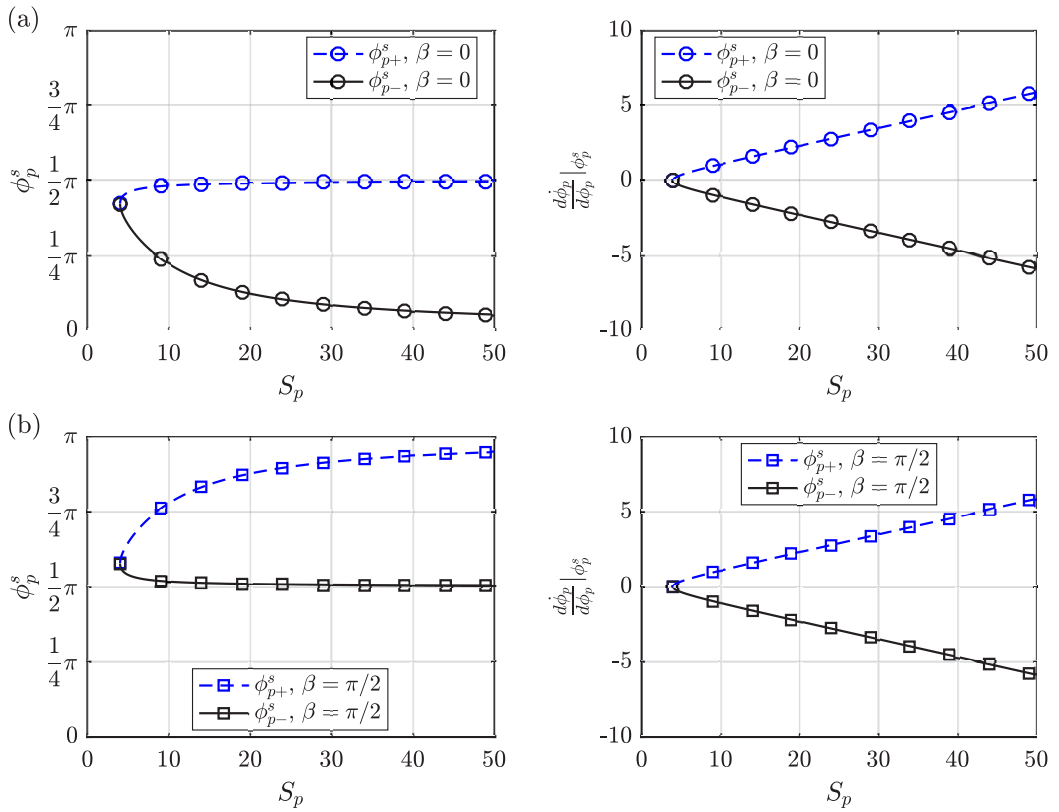

FIG. 3. Steady angles ϕ_p^s of the paramagnetic particle and the derivatives $\frac{d\dot{\phi}}{d\phi_p}|_{\phi_p^s}$ for field strength $S_p > S_p^{\rm cr}$, $r = 4$, and (a) $\beta = 0$ and (b) $\beta = \pi/2$.

determine that

$$t_p^{(0,\pi)} = \int_0^{\pi} \frac{d\phi_p}{\dot{\phi}_p} = \frac{r^2+1}{Q}\Bigg[\tanh^{-1}\left(\frac{S_p(\cos 2\beta + \sin 2\beta) - 1}{Q}\right) - \tanh^{-1}\left(\frac{S_p(\cos 2\beta - \sin 2\beta) + 1}{Q}\right) - \tanh^{-1}\left(\frac{S_p(\cos 2\beta + \sin 2\beta) + r^2}{Q}\right) - \tanh^{-1}\left(\frac{S_p(\sin 2\beta - \cos 2\beta) + r^2}{Q}\right)\Bigg], \tag{12}$$

where $Q = \sqrt{S_p^2 + S_p(r^2-1)\sin 2\beta - r^2}$. By definition, the period $t_p^{(0,2\pi)}$ is normalized by $\dot{\gamma}^{-1}$ in the above equation. When $S_p = 0$, the rotational period of the Jeffery orbit over $(0, 2\pi)$ is $t_0 = 2\pi(r + r^{-1})$ [13]. To examine the influence of the field strength and direction on the rotational period as compared to the Jeffery period, we plot a scaled period $\widetilde{T}_p = t_p^{(0,2\pi)}/t_0$ in Fig. 4 as a function of S_p and β. As can be observed, when $0 \leqslant \beta \leqslant \pi/2$, the period of rotation increases with an increase of S_p, i.e., the magnetic-field strength. By contrast, the period of rotation for $\pi/2 < \beta < \pi$ first decreases and then increases as S_p increases. For all β, the period of rotation approaches infinity as $S_p \to S_p^{\rm cr}$, i.e., the particle rotation is impeded.

The magnetic torque not only influences the rotational period, but also affects the symmetry property of the particle's rotational velocity. In the absence of a magnetic field, the rotational velocity of the particle is symmetric about $\phi = \pi/2$ according to Eq. (2) and thus the particle spends an equal

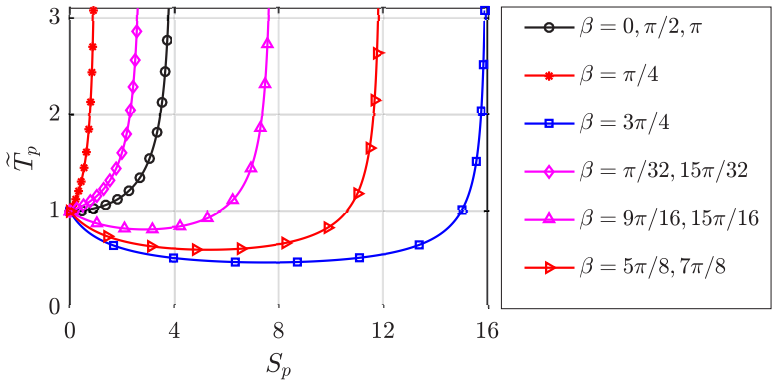

FIG. 4. Influence of magnetic-field strength S_p and direction β on the rotational period when $S_p < S_p^{\mathrm{cr}}$ and $r = 4$.

amount of time from $\phi = 0$ to $\pi/2$ and from $\pi/2$ to π. With an external (electric or magnetic) field, this characteristic can be modified. In an earlier study [13], symmetry breaking of the rotational velocity was reported for an electric field perpendicular to the flow direction, where the particle spent a longer time for the rotation from 0 to $\pi/2$ than that from $\pi/2$ to π.

In the present study, the direction of the magnetic field, characterized by the angle β, is arbitrary and its effect on the particle rotation needs to be understood. To characterize the symmetry or (asymmetry) of the rotational velocity about $\phi_p = \pi/2$, we have defined a ratio parameter τ_p in our earlier work [7]:

$$\tau_p = t_p^{(0,\pi/2)} \big/ t_p^{(0,\pi)}. \tag{13}$$

The value of τ_p was previously calculated by numerical integration [7]. In the present work, we obtain an analytical expression of $t_p^{(0,\pi)}$:

$$t_p^{(0,\pi/2)} = \frac{r^2+1}{Q}\left[\tanh^{-1}\left(\frac{S_p(\cos 2\beta + \sin 2\beta) + r^2}{Q}\right) - \tanh^{-1}\left(\frac{S_p(\cos 2\beta - \sin 2\beta) + 1}{Q}\right)\right]. \tag{14}$$

Substituting Eqs. (12) and (14) into Eq. (13) gives us an expression of τ_p. Based on this analytical expression, we find that when $\beta = \pi/4$ or $\beta = 3\pi/4$, $\tau_p = 0.5$, suggesting that a magnetic field that is applied at these two directions preserves the symmetry of the rotational velocity, despite that the rotational velocity and period are different, as shown in Fig. 4. For rotation from π to 2π, we can define a similar parameter τ_p' to characterize the symmetry of rotational velocity about particle orientation at $\phi_p = 3\pi/2$. It is noted that due to its periodicity dependence in π, the rotational velocity from π to 2π is the same as that from 0 to π and thus $\tau_p' = \tau_p$.

By definition, $\tau_p = 0.5$ represents that the rotational velocity is symmetric about $\phi_p = \pi/2$. Any τ_p values that deviate from 0.5 suggest asymmetric rotations. Figure 5 illustrates the effects of S_p and β on τ_p. Here we choose $S_p < 1$, so the particle is able to execute complete rotations for any $\beta \in (0, \pi)$, thus allowing us to examine the effect of β. We observe that $\tau_p > 0.5$ when $0 \leqslant \beta < \pi/4$ or $3\pi/4 < \beta \leqslant \pi$ [Fig. 5(a)] and $\tau_p < 0.5$ when $\pi/4 < \beta < 3\pi/4$ [Fig. 5(b)]. Moreover, τ_p becomes further away from 0.5 as S_p increases, meaning that the asymmetry of the rotational velocity is more prominent, because a larger S_p represents a stronger magnetic effect relative to the hydrodynamic effect.

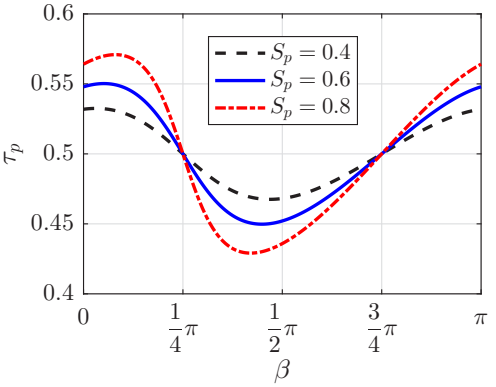

FIG. 5. Dependence of τ_p on β for a paramagnetic particle with field strength $S_p < 1$ and $r = 4$.

IV. FERROMAGNETIC PARTICLE

For a ferromagnetic particle, we assume that its magnetization $\mathbf{M}_0$ is parallel to its major axis, with M_0 denoting the magnitude of magnetization. Then the particle has a magnetic moment $\mathbf{m} = V\mathbf{M}_0 = VM_0(\sin\phi_f, 0, \cos\phi_f)$. The magnetic torque on a ferromagnetic particle can be written as $\mathbf{L}_{mf} = \mu_0 V(\mathbf{M}_0 \times \mathbf{H}_0) = L_{mf}\mathbf{e}_y$ and we obtain L_{mf} as

$$L_{mf} = -\mu_0 V M_0 H_0 \sin(\phi - \beta). \tag{15}$$

Taking a similar approach as the paramagnetic particle, we introduce a dimensionless parameter S_f to measure the relative strength between the magnetic and hydrodynamic torques on a ferromagnetic particle:

$$S_f = \frac{\mu_0 M_0 H_0 (r^2 D_{xx} + D_{zz})}{2\eta\dot{\gamma}}. \tag{16}$$

It is worth noting that S_f is nonzero for spherical particles ($r = 1$). This characteristic of the magnetic effect on spherical particles will be similar to that on ellipsoidal particles ($r > 1$), in clear contrast to paramagnetic particles.

When subjected to the flow and magnetic fields, the total dimensionless angular velocity of the ferromagnetic particle can be found,

$$\dot{\phi_f} = \frac{r^2\cos^2\phi_f + \sin^2\phi_f - S_f\sin(\phi_f - \beta)}{r^2 + 1}, \tag{17}$$

which shows that $\dot{\phi_f}$ is a periodic function of ϕ_f with period of 2π, in contrast to the angular velocity $\dot{\phi_p}$ of a paramagnetic particle in Eq. (7). We can define the critical field strength S_f^{cr} as the minimal S_f required to admit real solution(s) to $\dot{\phi_f} = 0$. However, analytical expressions of S_f^{cr} only exist for $\beta = 0$, $\pi/2$, π, and $3\pi/2$. Therefore, our analysis will focus on these special cases and will numerically analyze general cases for arbitrary β.

A. Critical field strength S_f^{cr}

Following lines similar to the paramagnetic case, we start with finding the impeded steady angle(s). Setting $\dot{\phi_f} = 0$ and assuming $\cos(\phi_f) \neq 0$, we can rewrite Eq. (17) as

$$a_4\left(\tan\phi_f^s\right)^4 + a_3\left(\tan\phi_f^s\right)^3 + a_2\left(\tan\phi_f^s\right)^2 + a_1\tan\phi_f^s + a_0 = 0, \tag{18}$$

where the coefficients $a_0 = r^4 - S_f^2 \sin^2\beta$, $a_1 = a_3 = S_f^2 \sin 2\beta$, $a_2 = 2r^2 - S_f^2$, and $a_4 = 1 - S_f^2 \cos^2\beta$. If $a_4 \neq 0$, Eq. (17) gives a quartic equation of $\tan(\phi_f)$. Solving it yields four solutions, i.e.,

$$\begin{aligned}\left[\tan\left(\phi_f^s\right)\right]_{1,2} &= -\frac{a_3}{4a_4} - w \pm \frac{1}{2}\sqrt{-4w^2 - 2p + \frac{q}{w}},\\ \left[\tan\left(\phi_f^s\right)\right]_{3,4} &= -\frac{a_3}{4a_4} + w \pm \frac{1}{2}\sqrt{-4w^2 - 2p - \frac{q}{w}},\end{aligned} \tag{19}$$

where

$$p = \frac{8a_4a_2 - 3a_3^2}{8a_4^2}, \quad q = \frac{a_3^3 - 4a_4a_3a_2 + 8a_4^2a_1}{8a_4^3}, \quad w = \frac{1}{2}\sqrt{-\frac{2p}{3} + \frac{1}{3a_4}\left(\kappa + \frac{\delta_0}{\kappa}\right)},$$

$$\kappa = \sqrt[3]{\frac{\delta_1 + \sqrt{\delta_1^2 - 4\delta_0^3}}{2}}, \quad \delta_0 = a_2^2 - 3a_1a_3 + 12a_0a_4,$$

$$\delta_1 = 2a_2^3 - 9a_1a_2a_3 + 27a_3^2a_0 + 27a_4a_1^2 - 72a_0a_2a_4.$$

The equation of $\tan(\phi_f^s)$ may degenerate to a cubic equation ($a_4 = 0$ but $a_3 \neq 0$) or a quadratic equation exists ($a_4 = a_3 = 0$). In such cases, the roots can be found analytically as well.

We now consider four special cases: $\beta = n\pi/2$ with $0 \leqslant n \leqslant 3$, for which S_f^{cr} can be analytically expressed. Setting $\dot{\phi}_f = 0$, we obtain the impeded steady angles as follows. For case A, $\beta = 0$, and case B, $\beta = \pi$,

$$\begin{aligned}\left(\tan\phi_f^s\right)_{1,2} &= \pm\sqrt{\frac{\left(S_f^2 - 2r^2\right) + S_f\sqrt{S_f^2 + 4r^2(r^2-1)}}{2\left(1 - S_f^2\right)}},\\ \left(\tan\phi_f^s\right)_{3,4} &= \pm\sqrt{\frac{\left(S_f^2 - 2r^2\right) - S_f\sqrt{S_f^2 + 4r^2(r^2-1)}}{2\left(1 - S_f^2\right)}}.\end{aligned} \tag{20}$$

In these cases, the critical field strength $S_f^{\mathrm{cr}} = 1$. For $S_f \geqslant S_f^{\mathrm{cr}}$, the real solutions $\tan(\phi_f^s)_{3,4}$ exist, whereas $\tan(\phi_f^s)_{1,2}$ are complex valued. For case C, $\beta = \pi/2$, and case D, $\beta = 3\pi/2$,

$$\begin{aligned}\left(\tan\phi_f^s\right)_{1,2} &= \pm\sqrt{\frac{\left(S_f^2 - 2r^2\right) + S_f\sqrt{S_f^2 - 4(r^2-1)}}{2}},\\ \left(\tan\phi_f^s\right)_{3,4} &= \pm\sqrt{\frac{\left(S_f^2 - 2r^2\right) - S_f\sqrt{S_f^2 - 4(r^2-1)}}{2}}.\end{aligned} \tag{21}$$

In these cases, the critical field strength

$$S_f^{\mathrm{cr}} = \begin{cases} 2\sqrt{r^2-1} & \text{if } r > \sqrt{2} \\ r^2 & \text{if } r \leqslant \sqrt{2}. \end{cases}$$

For $r > \sqrt{2}$, there are four solutions $(\tan\phi_f^s)_{1,2,3,4}$ if $S_f^{\mathrm{cr}} \leqslant S_f \leqslant r^2$ or two solutions $(\tan\phi_f^s)_{1,2}$ if $S_f > r^2$. For $r \leqslant \sqrt{2}$, there are always two solutions $[(\tan\phi_f^s)_{1,2}]$ if $S_f \geqslant S_f^{\mathrm{cr}}$. For each solution of $\tan\phi_f^s$, we can determine two values of ϕ_f^s, of which only one satisfies $\dot{\phi}_f = 0$ and is thus the true steady angle. By substituting the critical field strength into Eqs. (20) and (21), we can determine the

TABLE I. Summary of $S_f^{\rm cr}$ and $\phi_f^{\rm cr}$ for four special cases.

β	$S_f^{\rm cr}$ if $r \leqslant \sqrt{2}$	$\phi_f^{\rm cr}$ if $r \leqslant \sqrt{2}$	$S_f^{\rm cr}$ if $r > \sqrt{2}$	$\phi_f^{\rm cr}$ if $r > \sqrt{2}$
0	1	$\frac{\pi}{2}$	1	$\frac{\pi}{2}$
$\frac{\pi}{2}$	r^2	π	$2\sqrt{r^2-1}$	$\arctan(\pm\sqrt{r^2-2})+\pi$
π	1	$\frac{3\pi}{2}$	1	$\frac{3\pi}{2}$
$\frac{3\pi}{2}$	r^2	0	$2\sqrt{r^2-1}$	$\arctan(\pm\sqrt{r^2-2})+\pi$

critical steady angles $\phi_f^{\rm cr}$ for cases where the field is applied parallel or perpendicular to the flow direction. The critical field strength and corresponding critical steady angles for the special cases are summarized in Table I.

However, for arbitrary β, finding the critical field strength $S_f^{\rm cr}$ is not as straightforward as in Eq. (9), and it is impossible to find the analytical results for $S_f^{\rm cr}$. Here we use the bisection method (also known as the binary search method) to obtain the numerical solution of $S_f^{\rm cr}$, i.e., finding the smallest S_f such that there exists at least one real $(\tan\phi_f)_i$ (for $i = 1$, 2, 3, or 4) in Eq. (19). A numerical tolerance of 10^{-5} is used as the stop condition for finding $S_f^{\rm cr}$ by using the bisection method.

Figure 6(a) shows the value of $S_f^{\rm cr}$ as a function of β for different particle aspect ratios ($r = 1.4$, 2, 3, and 4). We can see that the field strength to impede the particle rotation is the smallest when $\beta = 0$, π, or 2π, at which $S_f^{\rm cr} = 1$, and the field strength to impede the rotation is the largest when $\beta = \pi/2$ or $3\pi/2$. In Fig. 6(b), when the field is applied at $\beta = 0$ ($\beta = \pi$), the particle will first be impeded at an angle of $\phi_f^{\rm cr} = \pi/2$ ($\phi_f^{\rm cr} = 3\pi/2$) for any particle aspect ratio. When the magnetic field is applied at $\beta = \pi/2$ or $3\pi/2$, the particle can be impeded at two different critical steady angles if $r > \sqrt{2}$. If $r \leqslant \sqrt{2}$, the particle is impeded at $\phi_f^{\rm cr} = \pi$ when $\beta = \pi/2$ or at $\phi_f^{\rm cr} = 0$ when $\beta = 3\pi/2$.

B. Steady angles in the strong field $S_f > S_f^{\rm cr}$

Similar to paramagnetic particles, a ferromagnetic particle cannot execute complete rotations and would be impeded at the steady angle(s) ϕ_f^s if the field strength $S_f > S_f^{\rm cr}$. The value of ϕ_f^s can be found from formulas in Eq. (19), which may exist as two, three, or four solutions depending on the particle aspect ratio r, S_f, and β. By using Eq. (19) and its degenerated forms, we map out the number

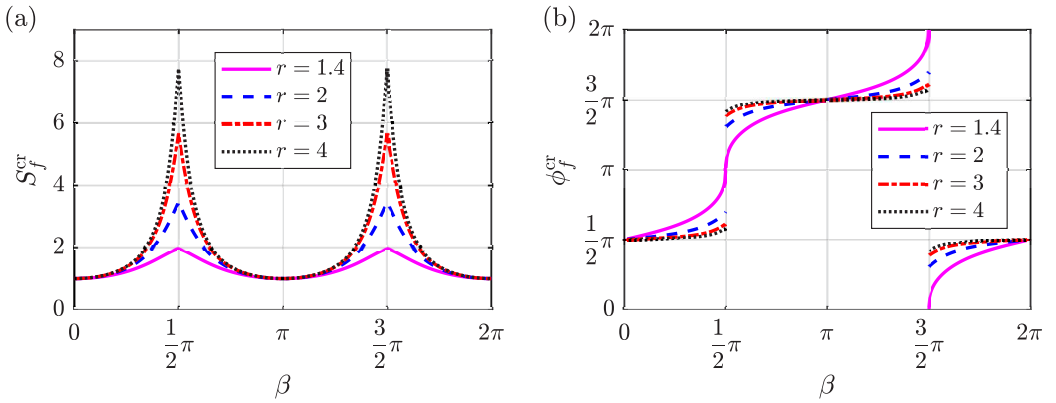

FIG. 6. (a) Critical-field strength $S_f^{\rm cr}$ and (b) critical steady angle $\phi_f^{\rm cr}$ as a function of field direction β for a ferromagnetic particle with $r = 1.4$, 2, 3, and 4.

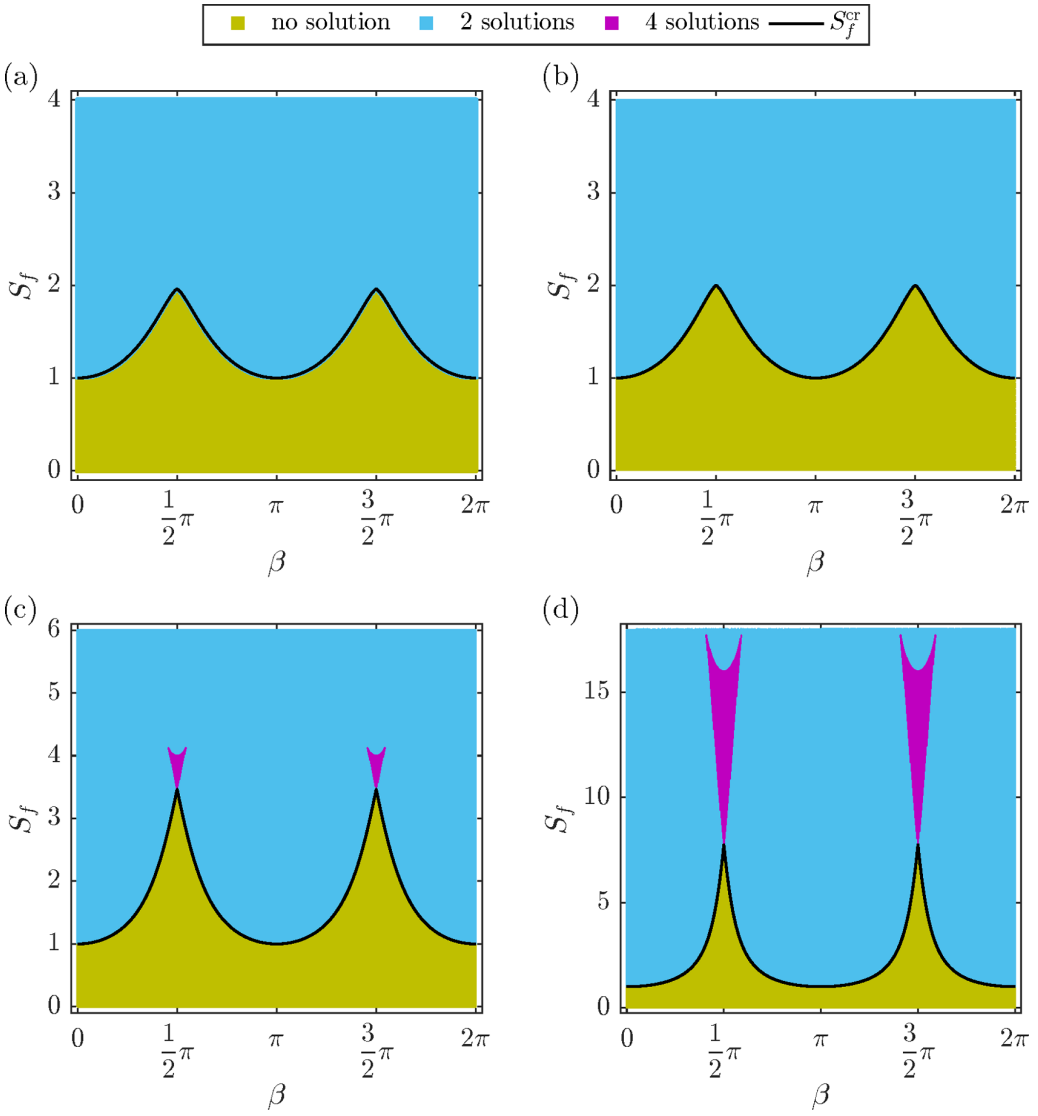

FIG. 7. Phase diagram of the number of steady angles for ferromagnetic particles for (a) $r = 1.4$, (b) $r = \sqrt{2}$, (c) $r = 2$, and (d) $r = 4$.

of steady angles (or solutions) over the parameter space of S_f and β for several different particle aspect ratios. Figure 7 shows that for $r > \sqrt{2}$, there are two regions near $\beta = \pi/2$ and $3\pi/2$ where there exist four steady angles. There are three solutions on the boundary between the two-solution and four-solution regions. When $S_f = S_f^{cr}$ there are two solutions if $\beta = \pi/2$ or $3\pi/2$, one solution for other values of β, and no solutions for $S_f < S_f^{cr}$. For $r \leqslant \sqrt{2}$, the particles can only have two solutions at most regardless of the field direction when $S_f > S_f^{cr}$ and one solution when $S_f = S_f^{cr}$. The stability of the impeded angles can be analyzed similarly by examining the derivatives $\frac{d\dot{\phi}_f}{d\phi_f}$ at $\phi_f = \phi_f^s$.

In Fig. 8, we present the result of the steady angles ϕ_f^s and their corresponding $\frac{d\dot{\phi}_f}{d\phi}$ for $\beta = 0$ and $\pi/2$, where the particle aspect ratio $r = 4$ (see additional figures in Appendix B for other β

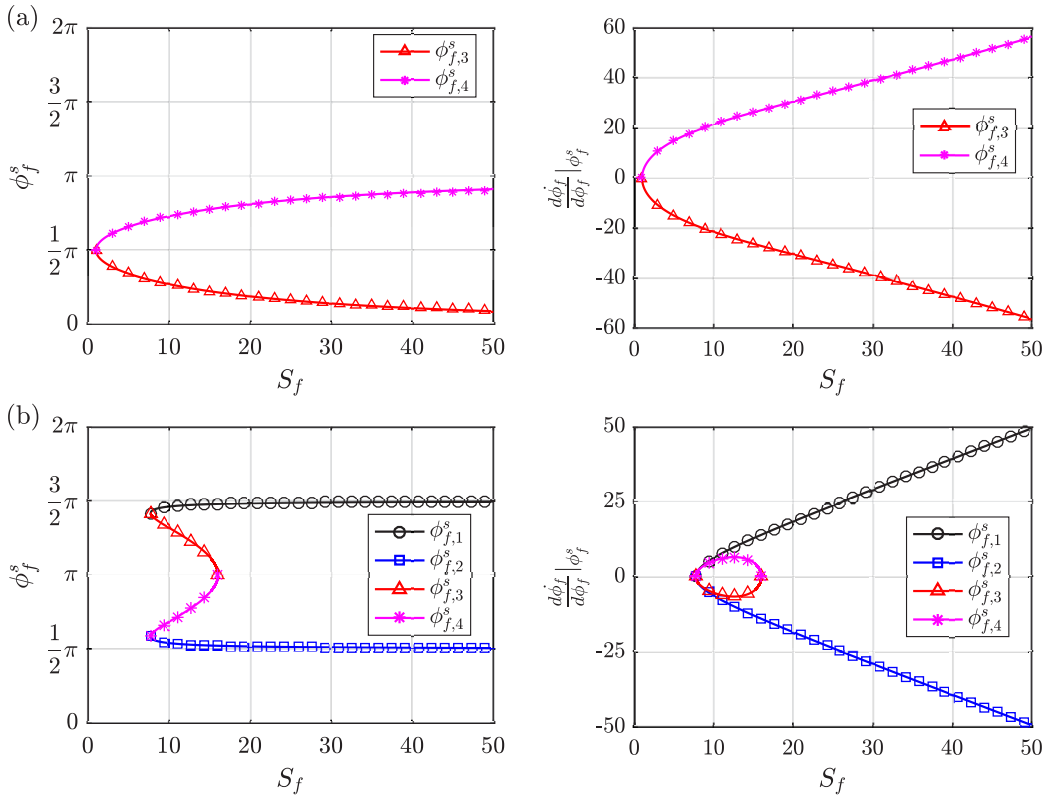

FIG. 8. Impeded angles ϕ_f^s of the ferromagnetic particle and derivatives $\frac{d\dot{\phi}_f}{d\phi_f}|_{\phi_f^s}$ for field strength $S_f > S_f^{\rm cr}$ and (a) $\beta = 0$ and (b) $\beta = \pi/2$. The particle aspect ratio is $r = 4$.

and particle aspect ratio $r = 1.4$). According to Fig. 8, we can observe several distinctive features. First, as $S_f \to \infty$, the particle will be impeded at two steady angles: One approaches β, i.e., the magnetization of the particle is parallel to the field direction, and the other approaches $\beta + \pi$ or $\beta - \pi$, i.e., the magnetization of the particle is antiparallel to the field direction. Of the two steady angles, the one with the magnetization parallel to the field (e.g., $\phi_{f,3}$ for $\beta = 0$ and $\phi_{f,2}$ for $\beta = \pi/2$) is stable, while the other is unstable. Second, when the magnetic field is applied parallel to the flow direction, i.e., $\beta = \pi/2$, the particle can be impeded at four steady angles, if $2\sqrt{r^2 - 1} < S_f < r^2$. Out of the four steady angles, two of them are stable and two of them are unstable. Similar results for $\beta = 3\pi/2$ are observed in Fig. 14 of Appendix B. Then the particle's eventual stable steady angle depends on its initial particle orientation. Similar to paramagnetic particles, when $S_f = S_f^{\rm cr}$, $\frac{d\dot{\phi}_f}{d\phi_f}|_{\phi_f^{\rm cr}} = 0$, suggesting that the $\phi_f^{\rm cr}$ is neutrally stable and would only be observed when there are no disturbances.

C. Particle rotation in the weak-field regime $S_f < S_f^{\rm cr}$

With a weak-field strength ($S_f < S_f^{\rm cr}$), the particle is able to perform periodic rotations, but its rotational period is altered by the magnetic field. Similarly, we define the dimensionless period of over a rotation 2π as $t_f^{(0,2\pi)}$ and introduce a scaled parameter $\widetilde{T}_f$ to measure the relative change of

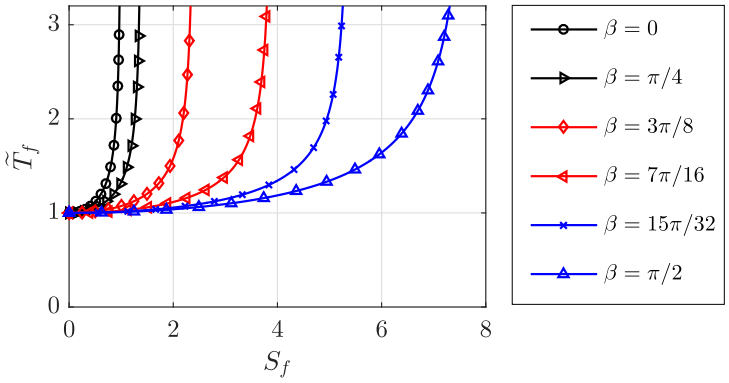

FIG. 9. Dimensionless period of particle rotational as a function of S_f for various magnetic field directions β.

the rotational period under the influence of an external uniform field,

$$\widetilde{T}_f = \frac{t_f^{(0,2\pi)}}{t_0} = \frac{1}{t_0}\int_0^{2\pi}\frac{d\phi_f}{\dot{\phi}_f} = \frac{1}{2\pi(r+r^{-1})}\int_0^{2\pi}\frac{r^2+1}{r^2\cos^2\phi_f + \sin^2\phi_f - S_f\sin(\phi_f-\beta)}d\phi_f. \tag{22}$$

Unlike the case of paramagnetic particles, there do not exist analytical expressions for $\widetilde{T}_f$ except for the special cases of β. Thus, we will numerically integrate $\widetilde{T}_f$ in Eq. (22) for general β. Figure 9 shows $\widetilde{T}_f$ as a function of S_f with a magnetic field applied at various β. Note that $\widetilde{T}_f$ is symmetric about $\pi/2$, i.e., $\widetilde{T}_f(\beta) = \widetilde{T}_f(\pi-\beta)$, and $\widetilde{T}_f$ is periodic in π, i.e., $\widetilde{T}_f(\beta) = \widetilde{T}_f(\pi+\beta)$. Therefore, the scaled period $\widetilde{T}_f$ is only plotted for $0 \leqslant \beta \leqslant \pi/2$. As can be observed, the period of rotation always increases with an increase of S_f, for any direction β, in contrast to the cases of paramagnetic particles. The period of particle rotation approaches infinity as $S_f \to S_f^{\mathrm{cr}}$, i.e., the particle rotation is impeded.

We now examine the effect of the magnetic field on the symmetry property of the particle's rotational velocity. The rotational velocity of a ferromagnetic particle has a period of 2π, as shown in Eq. (17). However, the ellipsoidal particle has a fore-aft symmetry, i.e., a periodicity of π. Therefore, we need to define two ratio parameters

$$\tau_{f,1} = t_f^{(0,\pi/2)}\big/t_f^{(0,\pi)}, \quad \tau_{f,2} = t_f^{(\pi,3\pi/2)}\big/t_f^{(\pi,2\pi)}. \tag{23}$$

By the above definitions, $\tau_{f,1}$ and $\tau_{f,2}$ characterize the symmetry of rotational velocity about $\phi_f = \pi/2$ for particle rotation $\phi_f \in [0,\pi]$ and about $\phi_f = 3\pi/2$ for rotation $\phi \in [\pi, 2\pi]$, respectively. To assess the role of β, we choose $S_f < 1$ so that the particle rotation is possible for any $\beta \in [0, 2\pi]$. As can be seen from Fig. 10, when the magnetic field is applied at $\beta = 0$ or π, $\tau_{f,1} = \tau_{f,2} = 0.5$, meaning that the rotational velocity is symmetric about $\phi_f = \pi/2$ and $3\pi/2$. This result can be further supported by the analytical expression of $t_f^{(0,\pi/2)}$ for $\beta = 0$ and π:

$$t_f^{(0,\pi/2)} = \frac{2(r^2+1)}{\sqrt{S^2+4r^2(r^2-1)}}\left\{\frac{1}{\sqrt{\xi_1^2-1}}\left[\frac{\pi}{2} - \arctan\left(\frac{\xi_1-1}{\sqrt{\xi_1^2-1}}\right)\right]\right.$$
$$\left. + \frac{1}{\sqrt{\xi_2^2-1}}\left[\frac{\pi}{2} + \arctan\left(\frac{\xi_2-1}{\sqrt{\xi_2^2-1}}\right)\right]\right\}, \tag{24}$$

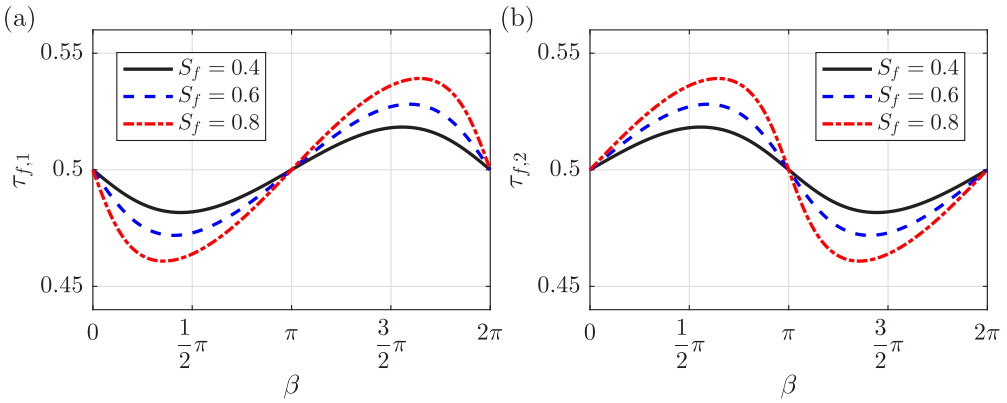

FIG. 10. Dependence of (a) $\tau_{f,1}$ and (b) $\tau_{f,2}$ on β for different field strengths $S_p < 1$ and $r = 4$.

where

$$\xi_{1,2} = \frac{-S\cos(\beta) \pm \sqrt{S^2 + 4r^2(r^2-1)}}{2(r^2-1)}. \tag{25}$$

Additionally, $t_f^{(\pi/2,\pi)} = t_f^{(0,\pi/2)}$ and thus $\tau_f = 0.5$. For $\beta \in (0, \pi)$, $\tau_{f,1} < 0.5$ and $\tau_{f,2} > 0.5$; for $\beta \in (\pi, 2\pi)$, $\tau_{f,1} > 0.5$ and $\tau_{f,2} < 0.5$.

V. LATERAL MIGRATION IN SHEAR FLOWS NEAR A SOLID WALL

Earlier studies have suggested two different mechanisms that can cause lateral migration of ellipsoidal magnetic particles in wall-bounded shear flows at low Reynolds number [6–8]. These studies focused on either paramagnetic [6,7] or ferromagnetic particles [8]. In a weak magnetic field, the asymmetry of the particle's rotational velocity is responsible for the lateral migration: It is experimentally shown that paramagnetic particles migrate away from a wall when $\tau > 0.5$, towards the wall when $\tau < 0.5$, and stay at a constant distance when $\tau = 0.5$. However, no study has been reported on lateral migration of ferromagnetic particles in this regime. On the other hand, in a strong magnetic field, the rotation of ferromagnetic particles is impeded and the particle assumes stable quasisteady angles. The stable orientation of the particle near a wall results in a nonzero lateral (or transverse) velocity, which is induced by the image stresslet due to the presence of a wall [8,10]. Depending on the steady angle, the particle can continuously translate away or towards the wall. However, lateral migration of paramagnetic particles in the strong-field regime has not been studied.

Our theoretical analysis has shown that the magnetic properties of the particle play a significant role in the rotational dynamics of a prolate spheroid in a simple shear flow and subject to a uniform magnetic field. By considering both weak- and strong-field regimes, we show that paramagnetic and ferromagnetic particles exhibit different rotational behaviors, in terms of symmetry of rotational velocity and impeded steady angles (see Secs. III and IV). While our analysis is performed on particles in a simple shear flow, the findings will qualitatively apply to particles in wall-bounded shear flows, although the wall and velocity profile will play additional roles. These theoretical insights can qualitatively inform us about the lateral migration motion when the particles are transported near a solid wall in shear flows.

In the following section, we use 2D numerical simulations to illustrate the implications of magnetic properties on the lateral migration of the particle in both weak- and strong-field regimes. Here we consider two common field directions $\beta = 0$ and $\beta = \pi/2$ and analyze and discuss the lateral migration of paramagnetic and ferromagnetic particles in different scenarios, in terms of parameter space of β, S_p, and S_f. As we will see, the numerical simulations, while developed in two dimensions

due to computational cost consideration, confirm the anticipated lateral migration behaviors as predicted by the theory. Thus, the numerical and analytical studies complement each other.

A. Numerical simulation

Our direct numerical simulation is based on the finite-element method and arbitrary Lagrangian-Eulerian method to solve for particle trajectory [19]. Similar methodologies have been successfully used by Hu *et al.* [20] and Ai *et al.* [21–23]. The numerical model couples the flow and magnetic fields and is implemented in COMSOL Multiphysics (see details in Appendix C). First, we use a stationary solver to calculate the magnetic field inside and outside the particle and compute the magnetic torque acting on the particle. Then the two-way coupling of the fluid-particle interaction model is solved by using a time-dependent solver and by importing the previously determined magnetic torque. Quadratic triangular elements are employed in the simulation. A fine mesh around the particle and a finer mesh around the tip of the particle are created to accurately calculate the hydrodynamic force and torque acting on the particle. After a grid independence test, about 12 000 and about 150 elements are used to discretize the fluid domain and particle surface, respectively. We validated the 2D numerical simulations by a comparison with the classical Jeffery theory in prior work [19]. Further, simulations with a magnetic field applied at $\beta = 0$ for particles in 2D simple shear flows showed good agreement with our theory.

We consider an elliptical particle ($r = 4$ and an equal-volume diameter $d = 7\ \mu$m) immersed in a plane Couette flow (see Fig. 16 in Appendix C). The lateral position of the particle is denoted by z_p and the particle is initially placed at $z_{p0} = 10\ \mu$m. Based on typical applications, we have the following estimates: external magnetic field $H_0 \sim O(10^3$–$10^5)$ A/m, particle size $a, b \sim O(10)\ \mu$m, fluid viscosity $\eta \sim O(10^{-3})$ Pa s, fluid density $\rho_f \sim O(10^3)$ kg/m^3, and shear rate $\dot{\gamma} \sim O(10^2)$ s^{-1}. It is reasonable to have $\chi \sim O(1)$ for paramagnetic particles and magnetization $M_0 \sim O(10^3)$ A/m for ferromagnetic particles. Based on these parameters, we have the flow Reynolds number $\mathrm{Re}_1 \lesssim O(1)$ and particle Reynolds number $\mathrm{Re}_2 \ll O(1)$. In our numerical simulations, the magnetic properties, magnetic-field strength, and fluid parameters are chosen to span the parameter space $S_p, S_f \sim O(10^{-1}$–$10^2)$ in order to examine particle migration in both weak- and strong-field regimes. It is known that the inertial effect can lead to lateral migration in shear flows [24,25]. In the simulations, we choose to use Reynolds numbers $\mathrm{Re}_1 \sim O(10^{-2})$ and $\mathrm{Re}_2 \sim O(10^{-4})$ to assess lateral migration which is largely due to the effect of the magnetic field.

B. Lateral migration in a weak field

In the weak-field regime, the particles are able to perform complete rotations while being transported by the shear flow. Here we plot the change of the lateral position normalized by the particle size $(z_p - z_{p0})/d$ over a rotation of 2π, as shown in Fig. 11. Comparison of the lateral migration between the two kinds of particles shows drastically different behaviors. The paramagnetic particle migrates away from the wall when the magnetic field is applied at $\beta = 0$ and towards the wall when $\beta = \pi/2$. In contrast, the ferromagnetic particle demonstrates zero net migrations over a rotation of 2π, when $\beta = 0$ or $\pi/2$.

The different lateral migration can be explained by the symmetry property of the rotational velocity according to Eq. (13) and Fig. 5 for paramagnetic particles and to Eq. (23) and Fig. 10 for ferromagnetic particles. When $\beta = 0$ (or $\beta = \pi/2$), the paramagnetic particles have $\tau_p > 0.5$ (or $\tau_p < 0.5$) for both rotations from $\phi_p = 0$ to π and $\phi_p = \pi$ to 2π, thus they continuously move upward (or downward); in contrast the ferromagnetic particles have $\tau_{f,1} < 0.5$ from $\phi_f = 0$ to π, thus moving downward, and then $\tau_{f,2} > 0.5$ from $\phi_f = \pi$ to 2π, thus moving upward. Furthermore, because $(\tau_{f,1} + \tau_{f,2})/2 = 0.5$, the upward and downward migration distances are approximately the same, leading to a zero net migration over a rotation of 2π. The distinctive migration behaviors suggest that using a*weak* field is a feasible way to separate these two kinds of magnetic particles. For instance, if $S = 0.664$ and $\beta = 0$, a paramagnetic particle ($r = 4$) moves in the lateral direction by $0.05d$, while

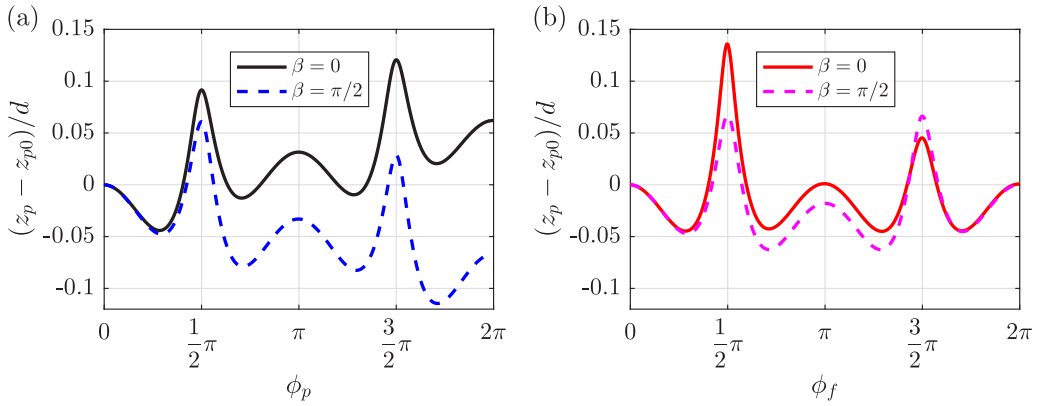

FIG. 11. Lateral migration of (a) paramagnetic and (b) ferromagnetic particles in the weak-field regime ($S_p \approx 0.664$ and $S_f \approx 0.664$) over a rotation of 2π with $r = 4$.

a ferromagnetic particle remains at the same lateral position after completing one cycle of rotation. Thus, for the paramagnetic particles to move by a lateral distance of d, it would take 20 rotational cycles, translating to a dimensionless time $\bar{t} = 20 t_0 \dot{\gamma} = 20 \frac{2\pi}{\dot{\gamma}}(r + 1/r)\dot{\gamma} = 40\pi(r + 1/r) \approx 500$.

C. Lateral migration in a strong field

In the strong-field regime, the magnetic torque is large enough to prevent particles from completing periodic rotations and the particles are pinned at steady angles. Under these circumstances, the stable orientation of the particle determines the lateral migration (or traverse) velocity [6–8]. Assuming that both paramagnetic and ferromagnetic particles are subject to the same dimensionless field strength, i.e., $S_p = S_f$, they will be pinned at different stable orientations, which can then lead to different lateral migration velocities. By adapting the far-field theory of Matsunaga *et al.* [8] into our analysis, the lateral migration velocity of the particles is related to the steady angle

$$U_{z,p} \approx C(r) d^3 \dot{\gamma} \frac{1}{z_p^2} \sin 2\phi_p^{ss}, \quad U_{z,f} \approx C(r) d^3 \dot{\gamma} \frac{1}{z_p^2} \sin 2\phi_f^{ss}, \tag{26}$$

where $U_{z,p}$ and $U_{z,f}$ are the lateral migration velocities, ϕ_p^{ss} and ϕ_f^{ss} are the stable steady angles, for paramagnetic and ferromagnetic particles, respectively, and $C(r)$ is a constant depending on the particle aspect ratio r. It has been shown numerically and theoretically that the sign of $\sin 2\phi_p^{ss}$ or $\sin 2\phi_f^{ss}$ determines the migration direction: Particles move away from the wall for $\sin 2\phi_p^{ss} > 0$ (or $\sin 2\phi_f^{ss} > 0$) [8].

Note that, although there may exist two or more steady angles, only the stable steady angles dictate the lateral migration (magnitude and direction) of ellipsoidal particles. According to Eqs. (11), (20), and (21) and our stability analysis in Secs. III and IV, we can write the stable steady angles for paramagnetic and ferromagnetic particles by substituting $\beta = 0$ and $\pi/2$. The explicit expressions are included here for convenience and clarity as follows:

$$\phi_{p,\beta=0}^{ss} = \arctan\left(S_p - \sqrt{S_p^2 - r^2}\right) \quad \text{if } S_p > r, \tag{27}$$

$$\phi_{p,\beta=\pi/2}^{ss} = \arctan\left(-S_p - \sqrt{S_p^2 - r^2}\right) + \pi \quad \text{if } S_p > r, \tag{28}$$

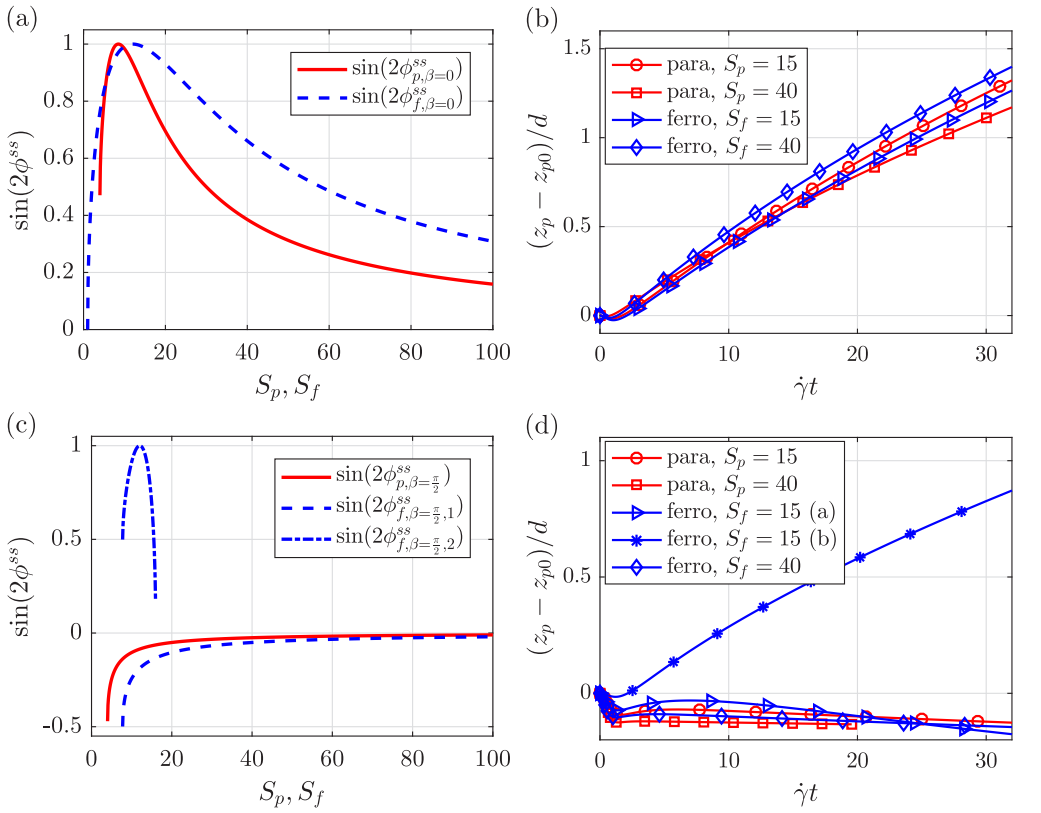

FIG. 12. Lateral migration of paramagnetic and ferromagnetic particles in a strong field with $r = 4$. (a) Theoretical values of $\sin(2\phi^{ss}_{p,\beta=0})$ (solid line) and $\sin(2\phi^{ss}_{f,\beta=0})$ (dashed line) for $\beta = 0$. (b) Lateral positions of the particles as a function of the dimensionless time $\dot{\gamma}t$ from the numerical simulations when $\beta = 0$. (c) Theoretical values of $\sin(2\phi^{ss}_{p,\beta=\pi/2})$ (solid line), $\sin(2\phi^{ss}_{f,\beta=\pi/2,1})$ (dashed line), and $\sin(2\phi^{ss}_{f,\beta=\pi/2,2})$ (dot-dashed line) for $\beta = \pi/2$. (d) Lateral positions of the particles as a function of the dimensionless time $\dot{\gamma}t$ from the numerical simulations when $\beta = \pi/2$. Depending on its initial orientation, the ferromagnetic particle shows two different lateral migration behaviors for $S_f = 15$.

$$\phi^{ss}_{f,\beta=0} = \arctan\left(\sqrt{\frac{\left(S_f^2 - 2r^2\right) - S_f\sqrt{S_f^2 + 4r^2(r^2-1)}}{2\left(1 - S_f^2\right)}}\right) \quad \text{if } S_f > 1, \tag{29}$$

$$\phi^{ss}_{f,\beta=\pi/2,1} = \arctan\left(-\sqrt{\frac{\left(S_f^2 - 2r^2\right) + S_f\sqrt{S_f^2 - 4(r^2-1)}}{2}}\right) + \pi \quad \text{if } S_f > 2\sqrt{r^2-1}, \tag{30}$$

$$\phi^{ss}_{f,\beta=\pi/2,2} = \arctan\left(\sqrt{\frac{\left(S_f^2 - 2r^2\right) - S_f\sqrt{S_f^2 - 4(r^2-1)}}{2}}\right) + \pi$$

$$\text{if } r > \sqrt{2},\ 2\sqrt{r^2-1} \leqslant S_f \leqslant r^2. \tag{31}$$

It is noted that for $r > \sqrt{2}$, there exist two possible stable steady angles $\phi^{ss}_{f,\beta=\pi/2,1}$ and $\phi^{ss}_{f,\beta=\pi/2,2}$ when $S_f^{\rm cr} \leqslant S_f \leqslant r^2$.

Figure 12(a) illustrates the characteristics of stable steady angles and lateral migration of particles in a strong field when $\beta = 0$. We can observe that $\sin 2\phi^{ss}_{p,\beta=0} < \sin 2\phi^{ss}_{f,\beta=0}$ except in a small interval of S_p, S_f, suggesting that ferromagnetic particles have a higher migration speed for most of the strong-field regime. Figure 12(b) shows the lateral position of the particles as a function of time from 2D numerical simulations for $\beta = 0$. Both the paramagnetic and ferromagnetic particles move away from the channel wall, in qualitative agreement with the theoretical prediction. Furthermore, it can be seen that the paramagnetic and ferromagnetic particles migrate away from the wall at similar speeds when $S_p = S_f = 15$, while the ferromagnetic particle moves faster when $S_p = S_f = 40$.

Figure 12(c) shows the characteristics of stable steady angles and lateral migration of particles in a strong field when $\beta = \pi/2$. Interestingly, the stable steady angles of the ferromagnetic particle can assume two possible values depending on the initial orientation of the particle for an intermediate-field strength, if the particle aspect ratio $r > \sqrt{2}$. As a result, the ferromagnetic particle can move either away from the wall or towards the wall. Such a prediction is confirmed by our numerical simulation by choosing different initial particle orientation, as shown in Fig. 12(d). In contrast, the paramagnetic particle always moves towards the wall due to $\sin 2\phi^{ss}_{p,\beta=\pi/2} < 0$.

The above findings suggest that it is also possible to separate paramagnetic and ferromagnetic particles by applying a *strong* magnetic field either perpendicular ($\beta = 0$) or parallel ($\beta = \pi/2$) to the flow direction. When $S = 15$ and $\beta = \pi/2$, it takes approximately a dimensionless time of 50 for a ferromagnetic particle to move laterally by a distance of d, while the paramagnetic particle only moves negligibly in the lateral direction. It is noted that when $S_p, S_f \to \infty$, the stable steady angles ϕ^{ss}_p and ϕ^{ss}_f both approach β; however, they approach β at different rates. It can be shown that when $\beta = 0$ and $\pi/2$, the value of $\sin 2\phi^{ss}_f / \sin 2\phi^{ss}_p \to 2$, suggesting a possible way to separate ferromagnetic and paramagnetic particles to this limit. However, with $S_p, S_f \to \infty$, the magnitude of lateral migration velocity will approach zero. Hence, when strong fields are used to separate ferromagnetic and paramagnetic particles, a field strength should be judiciously selected.

VI. CONCLUSION

We have investigated the rotational dynamics of paramagnetic and ferromagnetic ellipsoidal particles that are simultaneously subjected to a simple shear flow and a uniform magnetic field. We determined, analytically and numerically, the critical field strength of an arbitrarily directed magnetic field to impede particle rotations. When the field strength is larger than the critical strength, we determined the steady angles at which the particles are impeded and their stability was analyzed. The number of stable steady angles were examined based on the type and aspect ratio of the particle and the direction of the uniform magnetic field. When the field strength is smaller than the critical strength, we analyzed the effect of field direction on particle rotation, including the rotational period and the symmetry property of the particle's rotational velocity. Our findings show that the magnetic properties of the particles have a crucial role in the particle rotations and will result in drastically different lateral migration behaviors when the particles are transported in wall-bounded shear flows. By using numerical simulations, we investigated the particle lateral migration by imposing magnetic fields perpendicular and parallel to the flow direction. It was shown that in the weak-field regime, the paramagnetic particles move away from and towards the wall over a rotation of 2π, while the ferromagnetic particles exhibit negligible lateral migration. In the strong-field regime, paramagnetic and ferromagnetic particles migrate laterally at different velocities due to their difference in stable steady angles.

Our theory suggests several feasible ways to separate paramagnetic and ferromagnetic particles by applying magnetic fields either parallel or perpendicular to the flow. Successful separation is possible when S_f and S_p are both smaller than their respective critical field strengths. Separation is possible in a strong field when both kinds of particles are impeded from rotation, which can result

in different stable steady angles. In practical experimental settings, it is also possible to achieve separation by having one particle in the weak field and and the other in the strong field. Although the analysis was performed on a single particle, the results would apply to dilute suspensions as long as the particle-particle interactions is negligible. For example, in microfluidics applications, samples of interest often have low concentrations. Our work has great potential in bioseparations of magnetic biological entities, such as magnetobacteria which have permanent moments and biological cells which are labeled with magnetic beads.

ACKNOWLEDGMENTS

The authors gratefully acknowledge financial support from the Department of Mechanical and Aerospace Engineering, the Center for Biomedical Research at Missouri University of Science and Technology, and the Chancellor's Distinguished Fellowship (to C.A.S.).

APPENDIX A: STEADY ANGLES FOR PARAMAGNETIC PARTICLES

Here we show the steady angles of paramagnetic particles for $S_p > S_f^{\mathrm{cr}}$ when the magnetic field is applied in an arbitrary direction. Figure 13 shows that for $\beta = \pi/4$ and $\beta = 3\pi/4$, the steady angles demonstrates similar characteristics, as we discussed in the main text. Both ϕ_{p+}^s and ϕ_{p-}^s angles diverge from ϕ_p^{cr} into two branches, where ϕ_{p-}^s is stable and ϕ_{p+}^s is unstable. The major differences between the arbitrary cases and the $\beta = 0$ and $\beta = \pi/2$ cases are not only S_p^{cr} and ϕ_p^{cr} values, but also

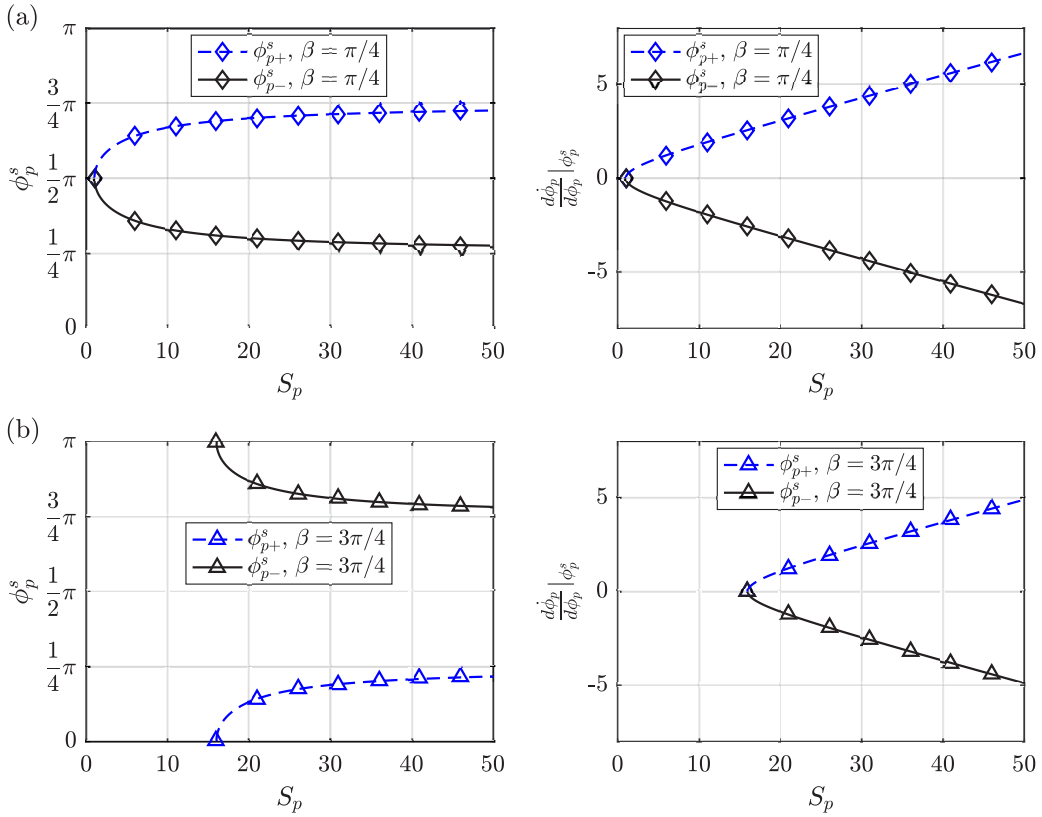

FIG. 13. Steady angles ϕ_p^s of the paramagnetic particle and the derivatives $\frac{d\dot{\phi}}{d\phi_p}|_{\phi_p^s}$ for field strength $S_p > S_p^{\mathrm{cr}}$, $r = 4$, and (a) $\beta = \pi/4$ and (b) $\beta = 3\pi/4$.

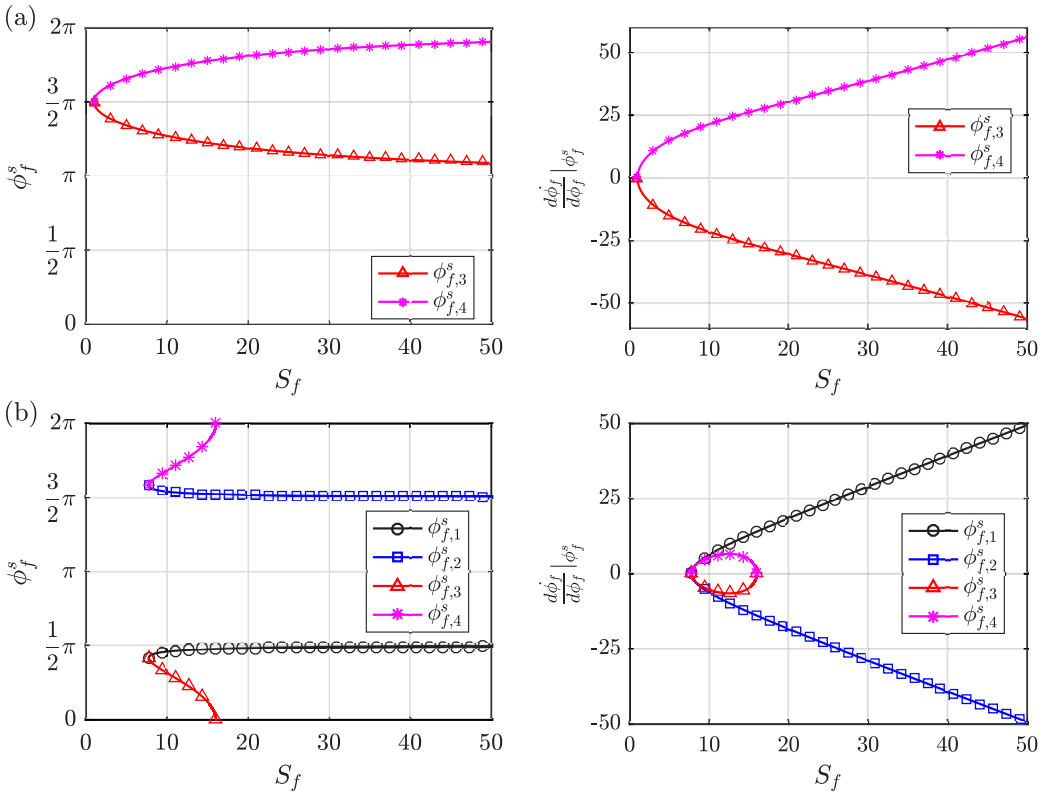

FIG. 14. Steady angles ϕ_f^s of the ferromagnetic particle and derivatives $\frac{d\dot{\phi}_f}{d\phi_f}|_{\phi_f^s}$ for field strength $S_f > S_f^{\rm cr}$ and (a) $\beta = \pi$ and (b) $\beta = 3\pi/2$. The particle aspect ratio is $r = 4$.

the rate at which ϕ_{p-}^s approaches β as S_p increases above $S_p^{\rm cr}$. In the limit of an infinite-field strength, the particle's major axis or minor axis can be aligned with the field direction, with the former being a stable configuration.

APPENDIX B: STEADY ANGLES FOR FERROMAGNETIC PARTICLES

Figure 14 shows the steady angles of a ferromagnetic particle and the corresponding derivatives, with $r = 4$ when $\beta = \pi$ and $3\pi/2$. Their behaviors are similar to those of the cases of $\beta = 0$ and $\pi/2$ in Fig. 8. It is noted that there exist two (when $S_f > r^2$), three (when $S_f = r^2$), or four (when $2\sqrt{r^2-1} < S_f < r^2$) steady angles when $\beta = 3\pi/2$.

Figure 15 plots the steady angles for a ferromagnetic particle with aspect ratio $r = 1.4 < \sqrt{2}$, when $\beta = 0, \pi/2, \pi$, and $3\pi/2$. For $S_f > S_f^{\rm cr}$, there are always two steady angles: $\phi_{f,3,4}$ when $\beta = 0$ and π, and $\phi_{f,1,2}$ when $\beta = \pi/2$ and $3\pi/2$. One of the two steady angles ($\phi_{f,3}$ and $\phi_{f,2}$) is the stable one.

APPENDIX C: NUMERICAL SIMULATION

We consider an elliptical particle ($r = 4$) immersed in a plane Couette flow, with a shear rate $\dot{\gamma} = 80\ {\rm s}^{-1}$, as shown in Fig. 16. The fluid is a Newtonian fluid with a density of 1000 kg/m^3 and dynamic viscosity of 0.1 Pa s. The density of the particle is 1000 kg/m^3. The equivalent diameter of the particle is $d = 7\ \mu$m. The size of the computational domain Ω is $w = 100\ \mu$m and $l = 800\ \mu$m. The particle surface is denoted by Γ. The Reynolds number of the flow ${\rm Re}_1 \approx \rho w^2 \dot{\gamma}/\mu = 8 \times 10^{-3}$

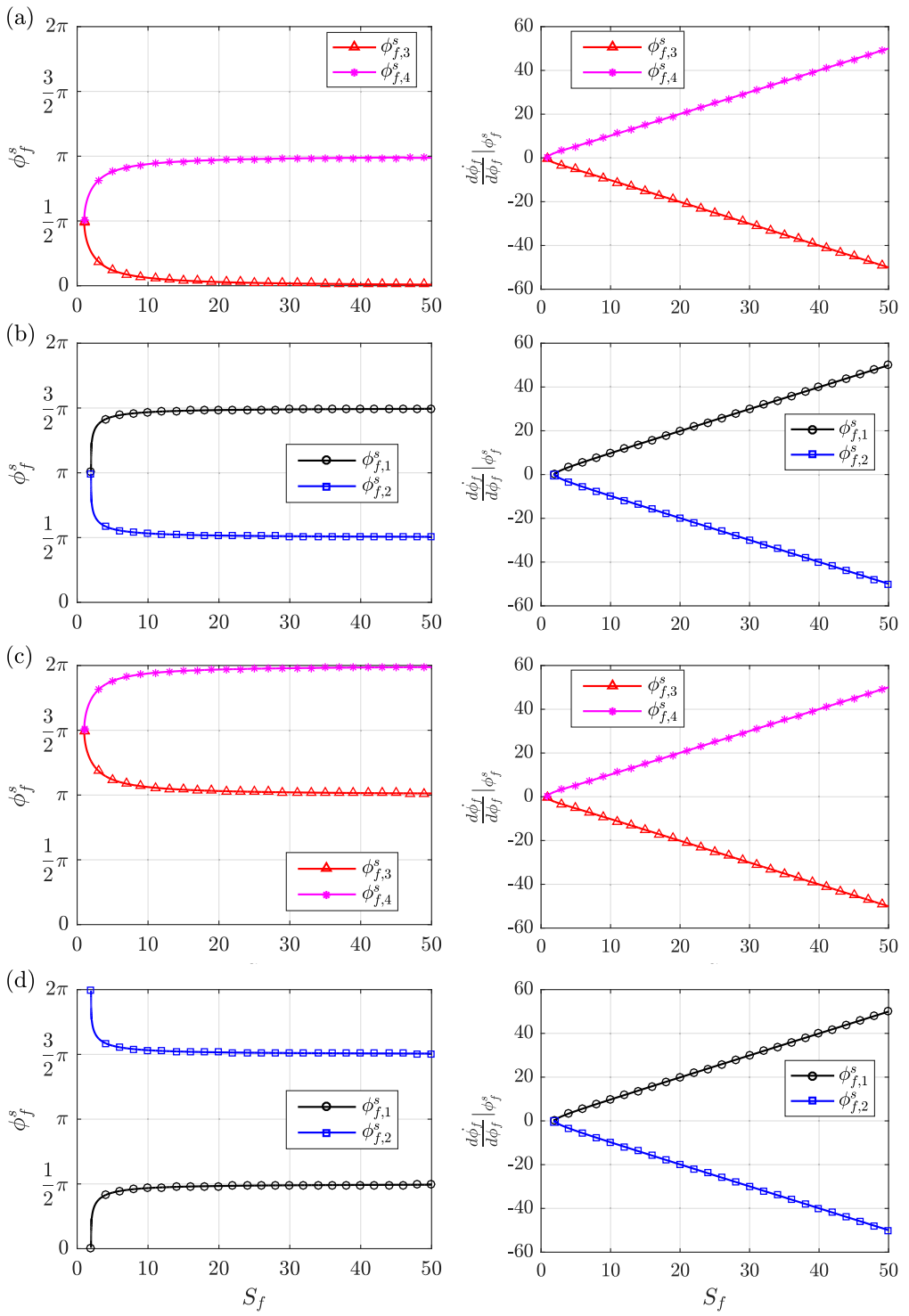

FIG. 15. Steady angles ϕ_f^s of a ferromagnetic particle with $r = 1.4$ and derivatives $\frac{d\dot{\phi}_f}{d\phi_f}|_{\phi_f^s}$ for field strength $S_f > S_f^{\text{cr}}$ and (a) $\beta = 0$, (b) $\beta = \pi/2$, (c) $\beta = \pi$, and (d) $\beta = 3\pi/2$.

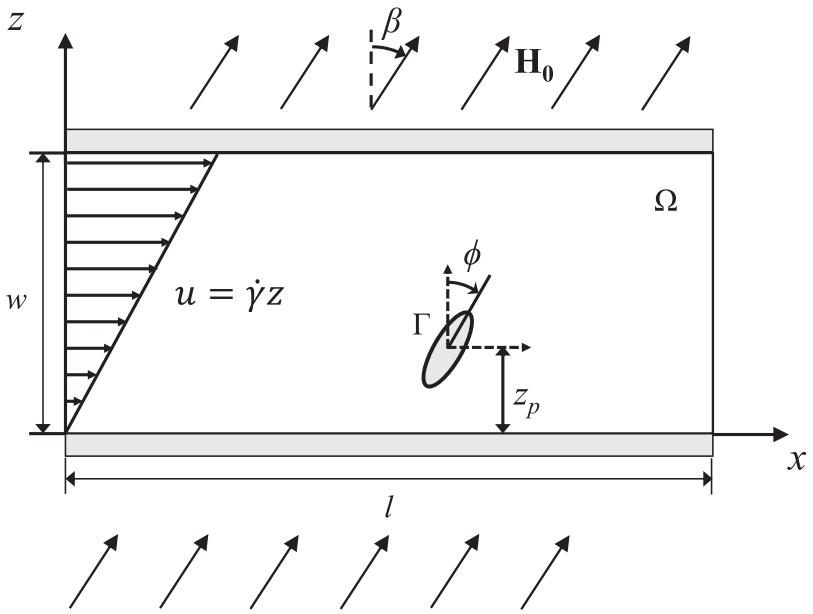

FIG. 16. Schematic of numerical model of an ellipsoidal particle suspended in a simple shear flow under the influence of a uniform magnetic field.

and the particle Reynolds number $\mathrm{Re}_2 \approx \rho d^2\dot{\gamma}/\mu = 8 \times 10^{-5}$, thus the effect of inertia is negligible. The lateral position of the particle is denoted by z_p. The orientation angle of the particle is denoted by ϕ. A uniform magnetic field $\mathbf{H}_0$ is imposed at an arbitrary direction, denoted by β.

The translation and rotation of particle in the x-z plane are governed by Newton's second law and Euler's equation

$$m_p \frac{d\mathbf{U}}{dt} = \mathbf{F}_h, \quad \mathbf{I}_p \frac{d\boldsymbol{\omega}}{dt} = \mathbf{L}_h + \mathbf{L}_m, \tag{C1}$$

where m_p and $\mathbf{I}_p$ are the mass and moment of inertia of the particle, $\mathbf{U}$ and $\boldsymbol{\omega}$ are the translational and rotational velocities of the particle, respectively, $\mathbf{F}_h$ is the hydrodynamic force, $\mathbf{L}_m$ is the magnetic torque, and $\mathbf{L}_h$ is the hydrodynamic torque. Note that $\boldsymbol{\omega} = \dot{\phi}\mathbf{e}_y$ for the in-plane rotational motion of the particle.

The coupling of the flow and magnetic fields is via the velocity boundary condition of the flow field on the particle surface, given by

$$\mathbf{u} = \mathbf{U} + \boldsymbol{\omega} \times (\mathbf{x}_s - \mathbf{x}_p), \tag{C2}$$

where $\mathbf{x}_s$ and $\mathbf{x}_p$ are the position vectors of the surface and the center of the particle. The hydrodynamic force and torque acting on the particle are given by

$$\mathbf{F}_h = \int (\boldsymbol{\sigma}_h \cdot \mathbf{n}) dS, \quad \mathbf{L}_h = \int [\boldsymbol{\sigma}_h \times (\mathbf{x}_s - \mathbf{x}_p) \cdot \mathbf{n})] dS, \tag{C3}$$

where $\boldsymbol{\sigma}_h$ is the hydrodynamic stress tensor acting on the surface of particle. The magnetic torque acting on the particle is $\mathbf{L}_m = \mu_0(\mathbf{m} \times \mathbf{H}_0)$. Given the initial position $\mathbf{C}(0)$ and initial orientation of the particle $\boldsymbol{\phi}(0) = \phi(0)\mathbf{e}_y$, the position of center $\mathbf{C}(t) = (x_p, z_p)$ and the orientation ϕ of particle are computed by

$$\mathbf{C}(t) = \mathbf{C}(0) + \int_0^t \mathbf{U}(s) ds, \quad \phi(t) = \phi(0) + \int_0^t \dot{\phi}(s) ds. \tag{C4}$$

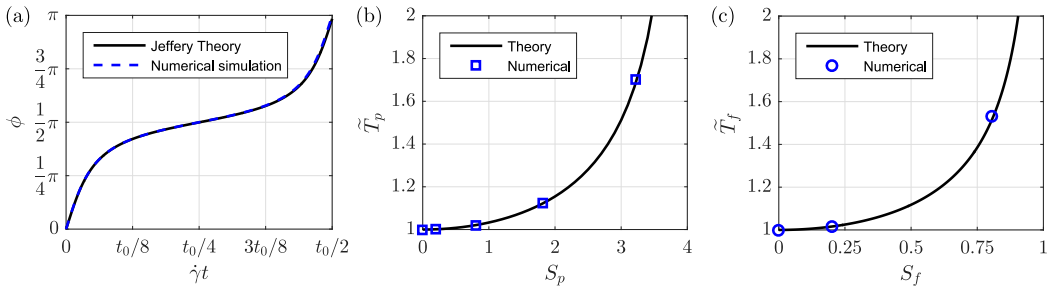

FIG. 17. Comparison between numerical simulations and theories: (a) particle rotation in a simple shear flow, (b) rotational period of paramagnetic particles in a magnetic field of $\beta = 0$, and (c) rotational period of ferromagnetic particles in a magnetic field of $\beta = 0$. A particle aspect ratio $r = 4$ is used in these comparisons.

It is known that 2D simulations can often give quantitatively different results from 3D simulations. However, in terms of identifying salient features of physics, similarities between 2D and 3D flows at low Reynolds number often outweigh their quantitative differences. In fact, 2D simulations of an elliptical particle in a simple shear flow have been shown to be able to accurately describe the in-plane rotational dynamics of a spheroidal ellipsoid in a 3D simple shear flow (see Ref. [26]). We validated the 2D numerical simulations by comparison with the classical Jeffery theory in prior work [19]. Further, simulations with a magnetic field applied at $\beta = 0$ for particles in 2D simple shear flows showed good agreement with our theory, as shown Fig. 17.

[1] J. Oberteuffer, Magnetic separation: A review of principles, devices, and applications, IEEE Trans. Magn. **10**, 223 (1974).
[2] C. Liu, T. Stakenborg, S. Peeters, and L. Lagae, Cell manipulation with magnetic particles toward microfluidic cytometry, J. Appl. Phys. **105**, 102014 (2009).
[3] J. Dobson, Magnetic nanoparticles for drug delivery, Drug Dev. Res. **67**, 55 (2006).
[4] L. Thiên-Nga, K. Hernadi, E. Ljubović, S. Garaj, and L. Forró, Mechanical purification of single-walled carbon nanotube bundles from catalytic particles, Nano Lett. **2**, 1349 (2002).
[5] G. Friedman and B. Yellen, Magnetic separation, manipulation and assembly of solid phase in fluids, Curr. Opin. Colloid Interface Sci. **10**, 158 (2005).
[6] R. Zhou, F. Bai, and C. Wang, Magnetic separation of microparticles by shape, Lab. Chip **17**, 401 (2017).
[7] R. Zhou, C. A. Sobecki, J. Zhang, Y. Zhang, and C. Wang, Magnetic control of lateral migration of ellipsoidal microparticles in microscale flows, Phys. Rev. Appl. **8**, 024019 (2017).
[8] D. Matsunaga, F. Meng, A. Zöttl, R. Golestanian, and J. M. Yeomans, Focusing and Sorting of Ellipsoidal Magnetic Particles in Microchannels, Phys. Rev. Lett. **119**, 198002 (2017).
[9] D. Matsunaga, A. Zöttl, F. Meng, R. Golestanian, and J. M. Yeomans, Far-field theory for trajectories of magnetic ellipsoids in rectangular and circular channels, J. Appl. Math. **83**, 767 (2018).
[10] J. Happel and H. Brenner, *Low Reynolds Number Hydrodynamics: With Special Applications to Particulate Media* (Springer Science + Business Media, New York, 2012), Vol. 1.
[11] N. Pamme, Magnetism and microfluidics, Lab. Chip **6**, 24 (2006).
[12] A. Okagawa, R. G. Cox, and S. G. Mason, Particle behavior in shear and electric fields. VI. The microrheology of rigid spheroids, J. Colloid Interface Sci. **47**, 536 (1974).
[13] R. S. Allan and S. G. Mason, Particle behavior in shear and electric fields. II. Rigid rods and spherical doublets, Proc. R. Soc. London Ser. A **267**, 62 (1962).

[14] S. T. Demetriades, Effect of electrostatic fields on the orientation of colloidal particles immersed in shear flow, J. Chem. Phys. **29**, 1054 (1958).
[15] Y. Almog and I. Frankel, The motion of axisymmetric dipolar particles in homogeneous shear flow, J. Fluid Mech. **289**, 243 (1995).
[16] G. B. Jeffery, The motion of ellipsoidal particles immersed in a viscous fluid, Proc. R. Soc. London Ser. A **102**, 161 (1922).
[17] J. A. Stratton, *Electromagnetic Theory* (Wiley, New York, 2007).
[18] I. Torres-Díaz and C. Rinaldi, Brownian dynamics simulations of ellipsoidal magnetizable particle suspensions, J. Phys. D **47**, 235003 (2014).
[19] J. Zhang and C. Wang, Numerical study of lateral migration of elliptical magnetic microparticles in microchannels in uniform magnetic fields, Magnetochem. **4**, 16 (2018).
[20] H. H. Hu, N. A Patankar, and M. Y. Zhu, Direct numerical simulations of fluid-solid systems using the arbitrary Lagrangian-Eulerian technique, J. Comput. Phys. **169**, 427 (2001).
[21] Y. Ai, S. W. Joo, Y. Jiang, X. Xuan, and S. Qian, Pressure-driven transport of particles through a converging-diverging microchannel, Biomicrofluidics **3**, 022404 (2009).
[22] Y. Ai, A. Beskok, D. T. Gauthier, S. W. Joo, and S. Qian, dc electrokinetic transport of cylindrical cells in straight microchannels, Biomicrofluidics **3**, 044110 (2009).
[23] Y. Ai, Z. Zeng, and S. Qian, Direct numerical simulation of ac dielectrophoretic particle-particle interactive motions, J. Colloid Interface Sci. **417**, 72 (2014).
[24] B. P. Ho and L. G. Leal, Inertial migration of rigid spheres in two-dimensional unidirectional flows, J. Fluid Mech. **65**, 365 (1974).
[25] J. Feng, H. H. Hu, and D. D. Joseph, Direct simulation of initial value problems for the motion of solid bodies in a Newtonian fluid. Part 2. Couette and Poiseuille flows, J. Fluid Mech. **277**, 271 (1994).
[26] J. Feng and D. D. Joseph, The unsteady motion of solid bodies in creeping flows, J. Fluid Mech. **303**, 83 (1995).